University of Zurich[UZH]

Zurich Open Repository and Archive
University of Zurich
University Library
Strickhofstrasse 39
CH-8057 Zurich
www.zora.uzh.ch

Year: 2020

Interferon- exposure induces a fragile glioblastoma stem cell phenotype with a transcriptional profile of reduced migratory and MAPK pathway activity

Lohmann, Birthe ; Silginer, Manuela ; Picard, Daniel ; Schneider, Hannah ; Remke, Marc ; Roth, Patrick ; Reifenberger, Guido ; Weller, Michael

Abstract: Background: Type I interferons (IFN- /) are cytokines that are typically expressed in response to double-stranded RNA associated with viral infections. Glioblastomas are the most common malignant primary brain tumors, characterized by an infiltrative growth pattern and prominent angiogenic activity, and thought to be maintained by a subpopulation of glioma-initiating (stem-like) cells (GICs). The growth of human GIC lines is highly sensitive to IFN- . Methods: Repetitive pulse stimulation with IFN- 1a (IS) was used to generate IS sublines that had acquired resistance to IFN- -induced suppression of sphere formation. These cell lines were characterized by analyses of type 1 IFN signaling, growth patterns, and transcriptomic profiles. Results: Here we report that repetitive IFN- 1a stimulation (IS) induces a stable phenotype (referred to as IS) at the level of maintaining sphere formation, although classical IFN signaling defined by the expression of both IFN receptors, myxovirus resistance protein A (MxA) accumulation, and STAT1 induction is unaffected. Furthermore, this stably altered IS phenotype is characterized by constitutively decreased sphere formation capacity and morphological features of senescence and autophagy. Transcriptional profiling reveals increased type I IFN signaling in these IS cells, but decreased expression of genes involved in receptor signaling and cell migration. Conclusions: Altogether, these data suggest a role for promoting IFN- signaling in glioblastoma and might provide clues to design future therapeutic approaches.

DOI: https://doi.org/10.1093/noajnl/vdaa043

Posted at the Zurich Open Repository and Archive, University of Zurich
ZORA URL: https://doi.org/10.5167/uzh-191413
Journal Article
Accepted Version

Originally published at:
Lohmann, Birthe; Silginer, Manuela; Picard, Daniel; Schneider, Hannah; Remke, Marc; Roth, Patrick; Reifenberger, Guido; Weller, Michael (2020). Interferon- exposure induces a fragile glioblastoma stem cell phenotype with a transcriptional profile of reduced migratory and MAPK pathway activity. Neuro-oncology advances, 2(1):vdaa043.
DOI: https://doi.org/10.1093/noajnl/vdaa043

Abstract

Background: Type I interferons (IFN-α/β) are cytokines that are typically expressed in response to double-stranded RNA associated with viral infections. Glioblastomas are the most common malignant primary brain tumors, characterized by an infiltrative growth pattern and prominent angiogenic activity, and thought to be maintained by a subpopulation of glioma-initiating (stem-like) cells (GIC). The growth of human GIC lines is highly sensitive to IFN-β.

Methods: Repetitive pulse stimulation with IFN-β1a (IS) was used to generate IS sublines that had acquired resistance to IFN-β-induced suppression of sphere formation. These cell lines were characterized by analyses of type 1 IFN signaling, growth patterns and transcriptomic profiles.

Results: Here we report that repetitive IFN-β1a stimulation (IS) induces a stable phenotype (referred to as IS) at the level of maintaining sphere formation, although classical IFN signaling defined by the expression of both IFN receptors, myxovirus resistance protein A (MxA) accumulation and STAT1 induction is unaffected. Furthermore, this stably altered IS phenotype is characterized by constitutively decreased sphere formation capacity and morphological features of senescence and autophagy. Transcriptional profiling reveals increased type I IFN signaling in these IS cells, but decreased expression of genes involved in receptor signaling and cell migration.

Conclusions: Altogether, these data suggest a role for promoting IFN-β signaling in glioblastoma and might provide clues to design future therapeutic approaches.

Importance of the study

Type I interferons (IFN-α/β) contribute to the natural immune response to viral infections, but have also recently been attributed anti-cancer stem stell properties. Glioblastomas are thought to be maintained by a subpopulation of glioma-initiating (stem-like) cells (GIC). The growth of human GIC lines is highly sensitive to IFN-β. We report that repetitive pulse exposure to IFN-β1a induces acquired resistance to IFN-β-induced suppression of sphere formation in GIC, despite preserved canonical type 1 IFN signaling (IS phenotype). Yet, IS GIC lines exhibit a fragile phenotype characterized by constitutively decreased spherogenicity, features of senescence, and a transcriptional profile of decreased expression of genes involved in receptor signaling and cell migration. These data suggest a role for promoting IFN-β signaling in the treatment of glioblastoma.

Keywords

Glioblastoma, interferon, stemness, signaling, transcription

Key points

Repetitive exposure to IFN-β induces an IS phenotype characterized by acquired resistance to IFN-β-induced suppression of sphere formation despite preserved canonical type 1 IFN signaling.

IS cells exhibited decreased growth and spherogenicity and a transcriptional profile of reduced migratory and MAPK pathway activity.

Introduction

Glioblastomas without mutations in the isocitrate dehydrogenase (IDH) 1 or 2 genes, i.e., IDH-wildtype glioblastomas are the most common and most malignant group of glial tumors. These tumors are characterized by a brain-infiltrative growth pattern, prominent angiogenic activity and variable patterns of molecular genetic changes in signaling and cell cycle-related pathways [1]. IDH-wildtype glioblastoma patients have a poor prognosis with a median survival in the range of 12 months in population-based studies [2,3] and of 14-17 months in contemporary clinical trials [4-6]. Besides surgery and radiotherapy, alkylating agent chemotherapy with temozolomide (TMZ) constitutes the standard treatment [7,8]. For at least two thirds of the patients, the DNA repair protein O^6-methylguanine-DNA methyltransferase (MGMT) antagonizes the effect of TMZ [9,10]. To overcome this challenge, interferon (IFN)-β1a treatment is of interest since it may sensitize human glioma cells, including glioma-initiating cells (GIC), to irradiation and TMZ [11,12].

IFN are pleiotropic cytokines that are divided into three classes. Type I IFN are a multi-member cytokine family consisting of around 20 members. The human genome contains IFN-α (13 subtypes), IFN-β, IFN-ε, IFN-κ and IFN-ω. They signal via the Janus-associated kinase-signal transducer and activator of transcription (JAK-STAT) cascade by binding to their cognate IFN-α/β receptor (IFNAR), IFNAR1 and IFNAR2. IFNAR1 associates with tyrosine kinase 2, and IFNAR2 with JAK1. This ligation leads to autophosphorylation of STAT members which translocate to the nucleus where they initiate transcription by binding specific sites in the promoter region of IFN-stimulated genes [13]. Type I IFN control innate and adaptive immunity as well as intracellular anti-microbial programs. They limit the dissemination of infectious agents like viral pathogens by induction of an antimicrobial state in infected cells and their

neighboring cells. They also modulate the immune system by promoting antigen presentation and natural killer cell function while suppressing pro-inflammatory pathways and cytokine production. Furthermore, type I IFN activate the adaptive immune system and thereby promote the development of T and B cell responses and immunological memory [13-15]. In addition, there is a growing body of evidence suggesting that type I IFN are also involved in natural and therapy-induced immunological control of malignancies that are not virus-related. However, the exact role of the type I IFN-mediated immune response to cancer is not fully understood [16]. Different studies indicate that type I IFN are involved in immunoediting [17,18], a process in which the immune system protects the host against oncogenesis and is able to recognize and respond to tumor development [19]. Furthermore, IFN-α/β have been proposed to mediate antitumoral effects, which are often delayed but enduring, by acting on cancer stem cells [20,21].

Type I IFN have been investigated for the treatment of multiple neoplasms, e.g. Kaposi sarcoma [22], hairy cell leukemia [16,23,24], renal cell carcinoma [25], chronic myeloid leukemia [26] and multiple myeloma [27,28]. Type I IFN were also tested in phase I/II clinical trials which suggested potential activity in newly diagnosed glioblastoma [29-31], yet, a recent randomized trial failed to confirm activity of type I IFN when added to the standard of care in newly diagnosed glioblastoma [32].

Resistance to conventional treatments like radio- and chemotherapy is considered a typical feature of GIC. Based on the establishment of models of acquired resistance to TMZ [33] and the profound anti-GIC properties of type I IFN [11], the present study explores the phenotypical changes and the underlying signaling perturbations caused by acquired resistance of GIC models to IFN. Here we report that, while such IFN resistance can indeed be induced, it comes at a price of a stable change in phenotype referred to here as “IFN-stimulated” (IS) that is characterized by impaired

tumor growth *in vitro* and *in vivo*, features of senescence and profound changes in gene expression related to receptor kinase signaling and cell migration.

Material and Methods

Materials and cell lines

Human IFN-β1a and pegylated IFN-β1a were provided by Biogen Inc. (Cambridge, MA). Stock solutions for *in vitro* experiments were prepared in 20 mM sodium acetate, pH 8.4, containing 150 mM arginine hydrochloride. 3-methyladenine was from Sigma Aldrich (St. Louis, MO). After informed consent and approval of the local ethics committees, the GIC lines were established from freshly resected tumors as described previously [34]. Cells were cultured in phenol red-free Neurobasal medium (NB) with B-27 supplement (20 µl/ml) (Thermo Fisher Scientific, Waltham, MA), L-glutamine (10 µl/ml), fibroblast growth factor-2 and epidermal growth factor (20 ng/ml each; Peprotech, Rocky Hill, PA). Temozolomide was provided by Merck (Lucerne, Switzerland). All cells were regularly tested for mycoplasma contamination and sent for short tandem repeat analysis (Deutsche Sammlung von Mikroorganismen and Zellkulturen - DSMZ, Braunschweig, Germany).

Generation of IFN-β1a resistant GIC

Samples of T-325, ZH-161, ZH-305 and S-24 cells were divided into two fractions indicated as GIC-NC for normal control GIC, which were not pulsed with IFN-β1a, or GIC-IS for GIC which were serially stimulated with IFN-β1a. Both cell fractions were continuously processed in parallel. These models were passaged in NB medium without or with IFN-β1a at the same time intervals. IS cells underwent serial IFN-β1a stimulation with 10 IU/ml for T-325 and 100 IU/ml for ZH-161, ZH-305 and S-24 every three to four weeks. After completion of more than four stimulation rounds, a sub-fraction of NC and IS cells were separated and seeded to assess their clonogenic

potential using spherogenicity assays. The remaining IS cells were kept in culture under permanent IFN-β1a stimulation as described above.

Real-time PCR, immunoblot, PCR and viability assay

Detailed methods are provided in Supplementary Note 1.

Gene expression profiling

500 ng total RNA was processed using the TruSeq RNA Sample Preparation v2 Kit (low-throughput protocol; Illumina, San Diego, CA) to prepare the barcoded libraries. Libraries were validated and quantified using DNA 1000 and high-sensitivity chips on a Bioanalyzer (Agilent, Böblingen, Germany); 7.5 pM denatured libraries were used as input into cBot (Illumina), followed by deep sequencing using HiSeq 2500 (Illumina) for 101 cycles, with an additional seven cycles for index reading. Fastq files were imported into Partek Flow (Partek, Chesterfield, MO). Quality analysis and control were performed on all reads to assess read quality and to determine the amount of trimming required (both ends: 13 bases 5´and 1 base 3´). Trimmed reads were aligned against the hg38 genome using the STAR - v2.5.3a aligner. Unaligned reads were further processed using Bowtie 2 v2.2.5 aligner. Aligned reads were combined before quantifying the expression using the Partek Expectation-Maximization algorithm against the ENSEMBL (release 84) database. Finally, statistical gene set analysis was performed using the T-test to determine differential expression at the gene level. Partek flow default settings were used in all analyses. For pathway analysis, gene sets were derived of curated pathways from several databases including GO, Reactome, KEGG (August 01, 2018 version; http://download.baderlab.org/EM_Genesets/current_release/Human/symbol/) and visualized using Cytoscape (www.cytoscape.org; $p \leq 0.001$, $q \leq 0.05$, similarity cutoff

0.5). RNA sequencing data were analyzed by cell line IS vs NC, and the T value was used to perform a ranked analysis.

Animal studies

The standard operating procedures for the animal studies were approved by the Swiss Cantonal Veterinary office under the Animal license permission number ZH105/2015. The care and treatment of all animals was in accordance with the Swiss Federal Law on the Protection of Animals of the Federal Food Safety and Veterinary Office and with the Swiss Federal Ordinance on the Protection of Animals. Following anesthesia, a burr hole was drilled in the skull 2 mm lateral to the bregma. The needle of a Hamilton syringe (Hamilton, Darmstadt, Germany) was introduced to a depth of 3 mm. A single cell suspension of 10^5 GIC in 2 µl PBS was slowly injected into the right striatum of immuno-compromised CD1 Foxn1 nude mice (Charles River, Sulzfeld, Germany) (n=10 per group). The mice enrolled had body weights of more than 20 g. Systemic treatment with human peg-IFN-β1a was performed by subcutanous injection twice weekly [$8x10^7$ U/kg]. The mice were observed daily and euthanized by cervical dislocation when developing neurological symptoms or at defined time points for histological analysis as indicated. Three mice per group were euthanized, defined by a pre-randomized list, when the third mouse in any group of the experiment became symptomatic in order to perform histological analysis to assess tumor growth at an early stage. The remaining mice were euthanized when displaying neurological symptoms to obtain survival data. All brains were explanted upon euthanasia, embedded in cryo moulds in Shandon Cytochrome yellow (Thermo Fisher Scientific) and frozen in liquid nitrogen. Tumor incidences and volumes were determined using hematoxylin and eosin stainings of 8 µm thick cryosections cut

using a Microm HM560 (Microchom HM560, Thermo Scientific) [35]. Details on immunohistochemistry methods are provided in Supplementary Note 2.

Data analysis

Data are representative of experiments performed two to three times with similar results. Statistical analysis was performed using GraphPad Prism 5 or 7 software. Statistical significance was assessed using either two-sided unpaired and paired Student's t-test or one-way ANOVA with Tukey's post hoc test for multiple analyses. Quantitative data are represented as mean ± standard deviation (SD) or standard error of the mean (SEM). A p value below 0.05 was considered significant. Kaplan Meier survival curves generated from the animal studies were analyzed using the Gehan-Breslow-Wilcoxon test. A p value below 0.05 was considered significant.

Results

Repeated exposure to IFN-β1a induces resistance in GIC

To model acquired resistance to IFN-β1a in GIC *in vitro*, T-325, ZH-161, ZH-305 or S-24 cells underwent serial IFN-β1a stimulation every three to four weeks (Figure 1A). To ascertain the induction of a stable, IFN-β1a-resistant phenotype, we determined clonogenic survival and assessed the half-maximal effective concentration (EC_{50}) of IS *versus* NC cells by metabolic activity assays. We noticed an up to eight-fold increase of the EC_{50} values in IS cells (Figure 1B). This resistance phenotype was maintained in all four IS lines (T-325-IS, ZH-161-IS, ZH-305-IS, S-24-IS) for twelve weeks after the last exposure to IFN-β1a. Later time points were not explored. Representative studies are shown in Figure S1A. Next, ZH-161-NC or ZH-161-IS cells were orthotopically implanted into nude mice which were treated biweekly with peg-IFN-β1a or vehicle control to explore whether IFN resistance established *in vitro* is maintained *in vivo*. First, we noted that there were more longer surviving mice in the untreated ZH-161-IS than in the untreated ZH-161-NC groups. Moreover, treatment with peg-IFN-β1a prolonged survival in ZH-161-NC glioma-bearing mice (***p=0.0001), but not in mice harboring ZH-161-IS gliomas (p=0.2712) (Figure 1D).

Classical type I IFN signaling is not affected in GIC-IS cells

We next explored the level of signaling at which resistance to IFN-β1a had evolved in IS cells. Both cognate receptors, IFNAR1 and IFNAR2, were expressed on NC and IS cells on mRNA (Figure 2A,B) and protein level (Figure 2C,D). Responsiveness to IFN-β1a was confirmed on the level of induction of STAT1 mRNA expression (Figure 2E). MxA as the classical downstream target of the IFN signaling cascade was also

concentration-dependently induced on mRNA (Figure 2F) and protein levels (Figure 2G) in NC and IS cells. The maintained signaling response to IFN was confirmed by a significant upregulation of MxA protein using immunohistochemistry in tumors of ZH-161-NC or ZH-161-IS glioma-bearing mice 48 h after peg-IFN-β1a treatment *in vivo* (Figure 2H).

Altered morphological and cell culture phenotype upon chronic IFN-β1a exposure

During culturing NC and IS cells in parallel, differences in proliferation were observed. While cell doubling times of NC and IS cells under optimal growth conditions were not different (Figure 3A), sphere formation defined as clusters of more than five cells was reduced in IS cells compared with NC cells. Further, sphere formation capacity was reduced in NC cells by IFN-β1a, whereas IFN-β1a had no such effect in IS cells (Figure 3B). A detailed evaluation of the size and morphology of spheres at day 20 revealed that untreated IS cells and IFN-β1a-treated NC cells generated smaller spheres than vehicle-treated NC cells (Figure S1B-D). Limiting dilution assays showed that IS cells had a growth disadvantage compared with NC cells (Figure 3C). When comparing cell cycle progression between NC and IS cells, no difference was observed besides an increased fraction of sub-G1 phase cells in IS cells, indicating spontaneous cell death (Figure 3D). We also noted a minor increase in the EC_{50} values for irradiation and temozolomide in the IS models, however, given their overall reduced growth rate relative to NC cells, we considered these data difficult to interpret and not indicative of induced cross-resistance. The previously reported sensitization of GIC to irradiation and temozolomide was no longer significant, but again this likely resulted mainly from overall reduced growth rates in the IS cultures (data not shown).

In vivo, the proliferation rate determined by Ki-67 labeling was significantly decreased only in peg-IFN-β1a-treated ZH-161-NC tumors, but not in peg-IFN-β1a-treated ZH-161-IS tumors (Figure 3E). Tumor vessel density studies did not show differences between the treatment groups and cell lines (Figure S2). To elucidate the impaired growth of IS cells, we investigated whether cell organelles were affected. Endoplasmatic reticula, Golgi apparatus and mitochondria of NC and IS cells appeared largely similar (Figure S3A). Next we determined senescence-associated β-galactosidase activity using irradiation at 20 Gy as a positive control [36]. IS cells uniformly exhibited higher β-galactosidase activity than NC cells (Figure 4A). In contrast, a single exposure to IFN-β did not induce β-galactosidase activity in NC cells (Figure S3B).

By electron microscopy, NC cells of ZH-161 and S-24 appeared unremarkable with intact plasma and nuclear membranes, well-separated nucleoli, physiological size and physiological distribution of mitochondria. Ribosomes were attached to the rough endoplasmatic reticula and numerous circular vesicles were detectable in the cyctoplasm (Figure 4B). In contrast, IS cells contained several autophagosomes filled with cellular components surrounded by double membrane layers, demonstrating the typical phenotype of autophagy [37]. GIC-NC were irradiated with 20 Gy as a positive control for senescence. Similar to IS cells, irradiated cells showed abundant autophagosomes and swollen mitochondria (Figure S4A). Yet, LC3 immunoblotting did not confirm constitutive activation of autophagy in IS cells (Figure S4B) and IS cells were not more sensitive to the inhibition of autophagy by 3-methyladenine than NC cells (Figure S4C).

In IS cells, rough endoplasmatic reticula were partially devoid of ribosomes, indicating impaired protein synthesis (Figure 4B). Given this depletion of ribosomes in IS cells, NC cells were also treated with cycloheximide, an inhibitor of protein

synthesis. Cycloheximide-treated NC cells showed a different phenotype compared to IS cells, exhibiting substantial amounts of intermediate filaments near the nucleus and mitochondria with dilated cristae and high electron negativity (Figure S4D). To gain support for an impaired protein synthesis, a protein synthesis assay was performed using cycloheximide-treated NC cells as a positive control. No difference between NC and IS cells became apparent (Figure S4E).

Transcriptional profiling of IS cells reveals downregulation of gene sets related to receptor signaling and cell migration

Whole transcriptome sequencing revealed profound changes in the transcriptional landscape in IS cells relative to the corresponding NC controls. Overall, 783 genes were significantly differentially expressed in both IS models *versus* the respective NC cells. Specifically, 578 and 205 genes were consistently upregulated or downregulated, respectively, in both ZH-161 and S-24 IS cells (Table S1, Figure S5A). Notably, unsupervised hierarchical clustering using the top 200 (Figure 5A) or all differentially expressed transcripts (Figure S5B) clearly segregated the models according to IS versus NC phenotype. Gene set enrichment analysis comparing the transcriptional profiles of both IS models with their NC GIC counterparts revealed upregulation of “interferon signaling” and “negative control of viral process”, likely reflecting the direct signaling activity of type I IFN (Figure 5B,C).

Up-regulation of the senescence marker, protein tyrosine phosphatase receptor type J (PTPRJ) [38], was consistent with the morphological observations in IS cells (Figure S5C). In addition, activating transcription factor (ATF) 4 signaling was upregulated in IS cells compared to NC cells. Although protein kinase RNA–like endoplasmic reticulum kinase (PERK)/eukaryotic translation initiation factor 2-alpha kinase 3 (EIF2AK3) were not differentially regulated between IS and NC cells, EIF2AK2, which

is typically upregulated during viral infections, was upregulated in IS cells (Figure S5D). Also, genes related to the terms *oxidative phosphorylation* (normalized enrichment score, NES, 1.67, p value 0), *mitochondrial gene expression* (NES 1.67, p value 0) and *hallmark unfolded protein response* (NES 1.45, p value 0.009) were positively enriched in IS cells (Table S2), but did not pass the false discovery rate threshold to be included in the gene set enrichment analysis.

One candidate gene induced in both IS models, nerve growth factor receptor (*NGFR*), was also induced in two other IS models not subjected to gene expression profiling (Figure S5E). Notably, the largest cluster downregulated in IS cells contained gene sets involved in receptor signaling. The top-ranking gene set among these affected signaling nodes was *transmembrane receptor protein tyrosine kinase activity* (NES -2.64, false discovery rate q value 4.79 x 10^{-04}). The transmembrane receptor protein tyrosine kinase, anaplastic lymphoma kinase (ALK), was the most significantly downregulated transcript (Table S1). Reduction of ALK mRNA and protein in IS cells was confirmed by RT-PCR and immunoblot (Figure S5F,G). Appropriate control experiments showed that a single exposure of either GIC line to IFN-β was insufficient to reduce ALK mRNA expression (data not shown). Hence, loss of ALK signaling activity may mediate part of the resistance to type I IFN.

Another cluster downregulated cluster in IS cells involved cell migration although genes in this cluster overlap with *receptor signaling* cluster. Migration-associated genes down-regulated in IS cells included IFITM1, DDX58 and LAMB1 (Figure 6). Accordingly, ZH-161 IS cells formed less invasive tumors than ZH-161 NC cells (Figure S6).

Discussion

The present study sought to explore biological consequences of chronic exposure of human glioblastoma stem cell models to type I IFN signaling. Repeated stimulation of GIC with IFN-β resulted in sublines referred to as IS that were refractory to the inhibitory effects of IFN on stemness defined by reduction of spherogenicity. IS cells generated by repetitive exposure to IFN-β1a remained insensitive to IFN-β1a-induced suppression of sphere formation for weeks (Figure 1, S1A) which could not be attributed to adaptive downregulation of canonical IFN signaling (Figure 2). Resistance to IFN-mediated growth suppression was maintained *in vivo* while canonical signaling was preserved there, too (Figure 1D, 2).

Cellular unresponsiveness to IFN has previously been analysed *in vitro* and *in vivo* in other cell types. Permanent stimulation with high-dose IFN or long-lasting peg-IFN led to downregulation of the IFNAR1 cell surface receptor in HEK-293T cells *in vitro* [39]. The state of unresponsiveness of IFN-treated cells lasted up to three days [40]. Once IFN was removed, IFNAR1 cell surface expression returned to control levels within three hours [39]. In addition, mice repeatedly treated with murine IFN-α became refractory to further IFN injection within hours after the first treatment by upregulating the ubiquitin-specific peptidase 18 (USP18) which has been described as a negative regulator of type I IFN signaling [41] and which was also upregulated in the IS models studied here (Figure 6).

Acquired resistance to IFN-β-induced growth suppression came at a price: the IS phenotype was characterized by decreased constitutive sphere formation, impaired growth under suboptimal conditions, and increased survival of tumor-bearing mice (Figure 1C, 3, S1B-D). Possible pathways induced by IFN-β and associated with decreased growth in IS cells include senescence [42] and autophagy [37] (Figure 4).

Senescence is a state in which viable cells cease to divide whereas autophagy is a catabolic process that degrades and recycles unnecessary or dysfunctional cellular components inside lysosomes. Both processes can be triggered by cytotoxic stress [43,44]. The phenotype of senescence can be heterogeneous and its expression depends on the exposed stress. It may comprise different effector mechanisms including autophagy, resistance to apoptosis, or activity of cyclin-dependent kinase inhibitors [45-47]. Metabolic or genotoxic stress-induced autophagy can have a survival effect rather than mediating cell death and allow a switch between apoptosis and senescence. Aging fibroblasts revealed some features of the IS phenotype such as increased β-galactosidase activity associated with increased number of autophagic vacuoles [48].

Plenty non-distinct fragmented membranes were also observed in IS cells which most likely originate from the rough endoplasmatic reticulum due to their shape and structure. Furthermore, rough endoplasmatic reticula without ribosomes attached were detected. Since ribosomes are associated with the translation of mRNA into protein [49], this might indicate impaired protein synthesis in IS cells (Figure 4B). When comparing IS cells to NC cells that were treated with CHX as a positive control for inhibited protein synthesis [50], CHX-treated NC still shared more morphological similarities with untreated NC than with untreated IS cells, suggesting that impaired protein synthesis in IS cells does not go along with morphological changes or that protein synthesis is not affected in IS cells to a relevant quantitative extent (Figure S4D). Increased expression of genes related to the unfolded protein response was confirmed by transcriptional profiling (Figure S5D,E).

RNA sequencing revealed profound changes in IS versus NC cells: maintained signaling activity of type I IFN was confirmed by demonstrating upregulation of genes related to *interferon signaling* and *negative control of viral process*es. In contrast,

among multiple gene families downregulated in IS cells, genes related to *tyrosine receptor signaling* and *cell migration* were of particular interest to understand the IS phenotype (Figure 5B). The profound changes in transcriptional profiles raise the possibility of durable epigenetic changes induced by type I IFN.

Altogether, these data indicate that prolonged exposure of human glioblastoma patients to type I IFN at sufficient local concentrations might be a suitable strategy to overcome treatment resistance. Local delivery might be a strategy to achieve this goal while circumventing systemic toxicity. Future studies should explore how to integrate IFN exposure with other novel treatment strategies, notably in the field of immunooncology.

Acknowledgement

The authors thank D. Baker and M. Naylor (both Biogen) for valuable discussions, and J. Friesen and F. Wiget for expert technical assistance.

Funding

This study was supported by the Swiss National Science Foundation (310030_166634/1, 310030_185155/1) and a research grant of Biogen (Cambridge, MA) to MW.

References

1. Louis DN, Perry A, Reifenberger G, et al. The 2016 World Health Organization Classification of Tumors of the Central Nervous System: a summary. *Acta Neuropathol.* 2016; 131(6):803-820.

2. Gramatzki D, Dehler S, Rushing EJ, et al. Glioblastoma in the Canton of Zurich, Switzerland revisited: 2005 to 2009. *Cancer.* 2016; 122(14):2206-2215.

3. Ostrom QT, Gittleman H, Liao P, et al. CBTRUS Statistical Report: Primary brain and other central nervous system tumors diagnosed in the United States in 2010-2014. *Neuro Oncol.* 2017; 19(suppl_5):v1-v88.

4. Chinot OL, Wick W, Mason W, et al. Bevacizumab plus radiotherapy-temozolomide for newly diagnosed glioblastoma. *The New England journal of medicine.* 2014; 370(8):709-722.

5. Gilbert MR, Dignam JJ, Armstrong TS, et al. A randomized trial of bevacizumab for newly diagnosed glioblastoma. *The New England journal of medicine.* 2014; 370(8):699-708.

6. Weller M, Butowski N, Tran DD, et al. Rindopepimut with temozolomide for patients with newly diagnosed, EGFRvIII-expressing glioblastoma (ACT IV): a randomised, double-blind, international phase 3 trial. *The Lancet. Oncology.* 2017; 18(10):1373-1385.

7. Weller M, van den Bent M, Tonn JC, et al. European Association for Neuro-Oncology (EANO) guideline on the diagnosis and treatment of adult astrocytic and oligodendroglial gliomas. *The Lancet. Oncology.* 2017; 18(6):e315-e329.

8. Stupp R, Mason WP, van den Bent MJ, et al. Radiotherapy plus concomitant and adjuvant temozolomide for glioblastoma. *The New England journal of medicine.* 2005; 352(10):987-996.

9. Hegi ME, Diserens AC, Gorlia T, et al. MGMT gene silencing and benefit from temozolomide in glioblastoma. *The New England journal of medicine.* 2005; 352(10):997-1003.

10. Hegi ME, Genbrugge E, Gorlia T, et al. MGMT Promoter Methylation Cutoff with Safety Margin for Selecting Glioblastoma Patients into Trials Omitting Temozolomide. A Pooled Analysis of Four Clinical Trials. *Clinical cancer research : an official journal of the American Association for Cancer Research.* 2018.

11. Happold C, Roth P, Silginer M, et al. Interferon-beta induces loss of spherogenicity and overcomes therapy resistance of glioblastoma stem cells. *Molecular cancer therapeutics.* 2014; 13(4):948-961.

12. Natsume A, Ishii D, Wakabayashi T, et al. IFN-beta down-regulates the expression of DNA repair gene MGMT and sensitizes resistant glioma cells to temozolomide. *Cancer research.* 2005; 65(17):7573-7579.

13. Platanias LC. Mechanisms of type-I- and type-II-interferon-mediated signalling. *Nature reviews. Immunology.* 2005; 5(5):375-386.

14. Pestka S, Krause CD, Walter MR. Interferons, interferon-like cytokines, and their receptors. *Immunological reviews.* 2004; 202:8-32.

15. Trinchieri G. Type I interferon: friend or foe? *J Exp Med.* 2010; 207(10):2053-2063.

16. Zitvogel L, Galluzzi L, Kepp O, Smyth MJ, Kroemer G. Type I interferons in anticancer immunity. *Nature reviews. Immunology.* 2015; 15(7):405-414.

17. Dunn GP, Bruce AT, Sheehan KC, et al. A critical function for type I interferons in cancer immunoediting. *Nat Immunol.* 2005; 6(7):722-729.

18. Koebel CM, Vermi W, Swann JB, et al. Adaptive immunity maintains occult cancer in an equilibrium state. *Nature.* 2007; 450(7171):903-907.

19. Schreiber RD, Old LJ, Smyth MJ. Cancer immunoediting: integrating immunity's roles in cancer suppression and promotion. *Science.* 2011; 331(6024):1565-1570.

20. Kayo H, Yamazaki H, Nishida H, Dang NH, Morimoto C. Stem cell properties and the side population cells as a target for interferon-alpha in adult T-cell leukemia/lymphoma. *Biochemical and biophysical research communications.* 2007; 364(4):808-814.

21. Moserle L, Indraccolo S, Ghisi M, et al. The side population of ovarian cancer cells is a primary target of IFN-alpha antitumor effects. *Cancer research.* 2008; 68(14):5658-5668.

22. Regnier-Rosencher E, Guillot B, Dupin N. Treatments for classic Kaposi sarcoma: a systematic review of the literature. *J Am Acad Dermatol.* 2013; 68(2):313-331.

23. Maevis V, Mey U, Schmidt-Wolf G, Schmidt-Wolf IG. Hairy cell leukemia: short review, today's recommendations and outlook. *Blood Cancer J.* 2014; 4:e184.

24. Quesada JR, Reuben J, Manning JT, Hersh EM, Gutterman JU. Alpha interferon for induction of remission in hairy-cell leukemia. *The New England journal of medicine.* 1984; 310(1):15-18.

25. Flanigan RC, Salmon SE, Blumenstein BA, et al. Nephrectomy followed by interferon alfa-2b compared with interferon alfa-2b alone for metastatic renal-cell cancer. *The New England journal of medicine.* 2001; 345(23):1655-1659.

26. Talpaz M, Kantarjian HM, McCredie K, Trujillo JM, Keating MJ, Gutterman JU. Hematologic remission and cytogenetic improvement induced by recombinant human interferon alpha A in chronic myelogenous leukemia. *The New England journal of medicine.* 1986; 314(17):1065-1069.

27. Mandelli F, Avvisati G, Amadori S, et al. Maintenance treatment with recombinant interferon alfa-2b in patients with multiple myeloma responding to conventional induction chemotherapy. *The New England journal of medicine.* 1990; 322(20):1430-1434.

28. Mellstedt H, Aahre A, Bjorkholm M, et al. Interferon therapy in myelomatosis. *Lancet.* 1979; 2(8144):697.

29. Groves MD, Puduvalli VK, Gilbert MR, et al. Two phase II trials of temozolomide with interferon-alpha2b (pegylated and non-pegylated) in patients with recurrent glioblastoma multiforme. *Br J Cancer.* 2009; 101(4):615-620.

30. Motomura K, Natsume A, Kishida Y, et al. Benefits of interferon-beta and temozolomide combination therapy for newly diagnosed primary glioblastoma with the unmethylated MGMT promoter: A multicenter study. *Cancer.* 2011; 117(8):1721-1730.

31. Wakabayashi T, Kayama T, Nishikawa R, et al. A multicenter phase I trial of combination therapy with interferon-beta and temozolomide for high-grade gliomas (INTEGRA study): the final report. *Journal of neuro-oncology.* 2011; 104(2):573-577.

32. Wakabayashi T, Natsume A, Mizusawa J, et al. JCOG0911 INTEGRA study: a randomized screening phase II trial of interferonbeta plus temozolomide in comparison with temozolomide alone for newly diagnosed glioblastoma. *Journal of neuro-oncology.* 2018; 138(3):627-636.

33. Happold C, Roth P, Wick W, et al. Distinct molecular mechanisms of acquired resistance to temozolomide in glioblastoma cells. *Journal of neurochemistry.* 2012; 122(2):444-455.

34. Le Rhun E, von Achenbach C, Lohmann B, et al. Profound, durable and MGMT-independent sensitivity of glioblastoma cells to cyclin-dependent kinase inhibition. *International journal of cancer. Journal international du cancer.* 2018.

35. Schneider H, Lohmann B, Wirsching HG, et al. Age-associated and therapy-induced alterations in the cellular microenvironment of experimental gliomas. *Oncotarget.* 2017; 8(50):87124-87135.

36. Fumagalli M, Rossiello F, Mondello C, d'Adda di Fagagna F. Stable cellular senescence is associated with persistent DDR activation. *PLoS One.* 2014; 9(10):e110969.

37. Boya P, Codogno P, Rodriguez-Muela N. Autophagy in stem cells: repair, remodelling and metabolic reprogramming. *Development.* 2018; 145(4).

38. Althubiti M, Lezina L, Carrera S, et al. Characterization of novel markers of senescence and their prognostic potential in cancer. *Cell Death Dis.* 2014; 5:e1528.

39. Marijanovic Z, Ragimbeau J, Kumar KG, Fuchs SY, Pellegrini S. TYK2 activity promotes ligand-induced IFNAR1 proteolysis. *Biochem J.* 2006; 397(1):31-38.

40. Larner AC, Chaudhuri A, Darnell JE, Jr. Transcriptional induction by interferon. New protein(s) determine the extent and length of the induction. *The Journal of biological chemistry.* 1986; 261(1):453-459.

41. Sarasin-Filipowicz M, Wang X, Yan M, et al. Alpha interferon induces long-lasting refractoriness of JAK-STAT signaling in the mouse liver through induction of USP18/UBP43. *Mol Cell Biol.* 2009; 29(17):4841-4851.

42. Lee BY, Han JA, Im JS, et al. Senescence-associated beta-galactosidase is lysosomal beta-galactosidase. *Aging Cell.* 2006; 5(2):187-195.

43. Serrano M, Lin AW, McCurrach ME, Beach D, Lowe SW. Oncogenic ras provokes premature cell senescence associated with accumulation of p53 and p16INK4a. *Cell.* 1997; 88(5):593-602.

44. Young AR, Narita M. Connecting autophagy to senescence in pathophysiology. *Curr Opin Cell Biol.* 2010; 22(2):234-240.

45. Hernandez-Segura A, Nehme J, Demaria M. Hallmarks of Cellular Senescence. *Trends Cell Biol.* 2018; 28(6):436-453.

46. Patschan S, Chen J, Polotskaia A, et al. Lipid mediators of autophagy in stress-induced premature senescence of endothelial cells. *Am J Physiol Heart Circ Physiol.* 2008; 294(3):H1119-1129.

47. Young AR, Narita M, Ferreira M, et al. Autophagy mediates the mitotic senescence transition. *Genes Dev.* 2009; 23(7):798-803.

48. Gerland LM, Peyrol S, Lallemand C, Branche R, Magaud JP, Ffrench M. Association of increased autophagic inclusions labeled for beta-galactosidase with fibroblastic aging. *Exp Gerontol.* 2003; 38(8):887-895.

49. Savir Y, Tlusty T. The ribosome as an optimal decoder: a lesson in molecular recognition. *Cell.* 2013; 153(2):471-479.

50. Roth W, Fontana A, Trepel M, Reed JC, Dichgans J, Weller M. Immunochemotherapy of malignant glioma: synergistic activity of CD95 ligand and chemotherapeutics. *Cancer Immunol Immunother.* 1997; 44(1):55-63.

Figure Legends

Figure 1. **Responsiveness to IFN-β1a in NC and IS cells *in vitro*.** A. Schematic illustration of the generation of "interferon-stimulated" (IS) cells. B. Clonogenic survival of normal control (NC) or IS cells upon IFN-β1a stimulation was assessed by MTT assay. C. Nude mice intracranially implanted with ZH-161-NC or ZH-161-IS cells were treated twice weekly with vehicle or peg-IFN-β1a [$8x10^7$ U/kg] from day 14 on. Kaplan-Meier survival curves of ZH-161-NC or ZH-161-IS glioma-bearing mice are shown (median survival in days provided in brackets, Gehan-Breslow-Wilcoxon test, $p<0.05$, n=7-8 mice per group).

Figure 2. **Classical type I IFN signaling in IS versus NC cells *in vitro* and *in vivo*.** A-D. NC or IS cells were studied for IFNAR1 and IFNAR2 mRNA expression by RT-PCR (A,B). Protein levels of IFNAR1 (C) and IFNAR2 (D) were analyzed by cell surface flow cytometry. Specific fluorescence indexes (SFI) are indicated in the upper right corner. E-G. Responsiveness to IFN-β1a (24 h) was assessed at the level of STAT1 (E) and MxA (F) gene expression by RT-PCR and protein accumulation by immunoblot (G). ARF-1 served as a housekeeping gene for RT-PCR and actin served as loading control in immunoblots. H. Brain sections of ZH-161-NC or ZH-161-IS tumor-bearing animals sacrificed when the third mouse became symptomatic were immunohistochemically stained for MxA protein. Data are expressed as mean and SEM (***$p<0.001$, one way ANOVA with Tukey's post hoc test for multiple analysis, peg-IFN-β1a versus vehicle treatment). Scale bars of full pictures correspond to 100 μm, scale bars of inserts to 25 μm.

Figure 3. **Chronic IFN-β1a exposure induces an altered phenotype in IS cells.** A. Cell doubling times of NC versus IS cells under optimal growth conditions. B. Responsiveness to IFN-β1a (100 IU/ml) was determined by obtaining sphere counts of ZH-305-NC and ZH-305-IS on day 20. Data are expressed as mean and SEM (one way ANOVA with Tukey's post hoc test for multiple analysis, ***p<0.001 IFN-β1a-treated versus untreated cells, $^{+++}$p<0.001 IS versus NS cells). C. Sphere formation of ZH-161 and S-24-NC (white) or IS (black) cells after seeding different cell densities. Metabolic activity was assessed by MTT assay. D. Proportions of cell cycle distribution of NC versus IS cells (black = sub-G1, dark grey = G0/G1, light grey = S, white = G2 phase). E. Proliferation was analyzed by determining the percentage of Ki-67-positive tumor cell nuclei in ZH-161-NC or ZH-161-IS tumor-bearing mice. Data are expressed as mean and SEM (***p<0.001, one way ANOVA with Tukey's post hoc test for multiple analysis, peg-IFN-β1a versus vehicle treatment). Scale bars of full pictures correspond to 100 µm, scale bars of inserts to 25 µm.

Figure 4. **Morphological characteristics of GIC-IS.** A. Senescence-associated β-galactosidase staining on cytospins of untreated NC or IS cells, using irradiated NC cells (20 Gy, 5 days) as a positive control. Scale bars of full picture corresponds to 100 µm, scale bars of insert correspond to 25 µm. Data are expressed as mean percentages and SEM of stained cells (***p<0.001, one way ANOVA with Tukey's post hoc test for multiple analysis, IS or irradiated cells versus NC cells) B. Transmission electron microscopy features of ZH-161 and S-24 NC versus IS cells. Representative pictures of 70 nm sections are shown. V = vesicle (B1), M = mitochondria (B1, B2), asterisk = rough endoplasmatic reticulum (B1-B4), AP = autophagosome (B3, B4), arrow = non-distinct fragmented membranes (B4).

Figure 5. **Gene expression profiling of the IS phenotype.** A. Unsupervised hierarchical clustering using the top 200 genes. Upregulated genes are indicated in red, downregulated genes in green (Z score +/- 2). B. Visualization of the gene set enrichment analysis of ZH-161 and S-24 IS versus NC cells. Each dot indicates a gene set. Blue dots indicate a positive enrichment in IS cells, red dots refer to a negative enrichment in IS cells. The size of the dots corresponds to the number of genes present (for details, see Methods).

Figure 6. **Gene expression profiling of the IS phenotype in both models combined.** Unsupervised hierarchical clustering of the most differentially regulated genes in both models combined. Upregulated genes are indicated in red, downregulated genes in green (Z score +/- 2). Genes involved in IFN signaling are marked in light blue. Genes associated with negative regulation of viral processes are labelled in dark blue. Genes referring to cell migration are indicated in purple.

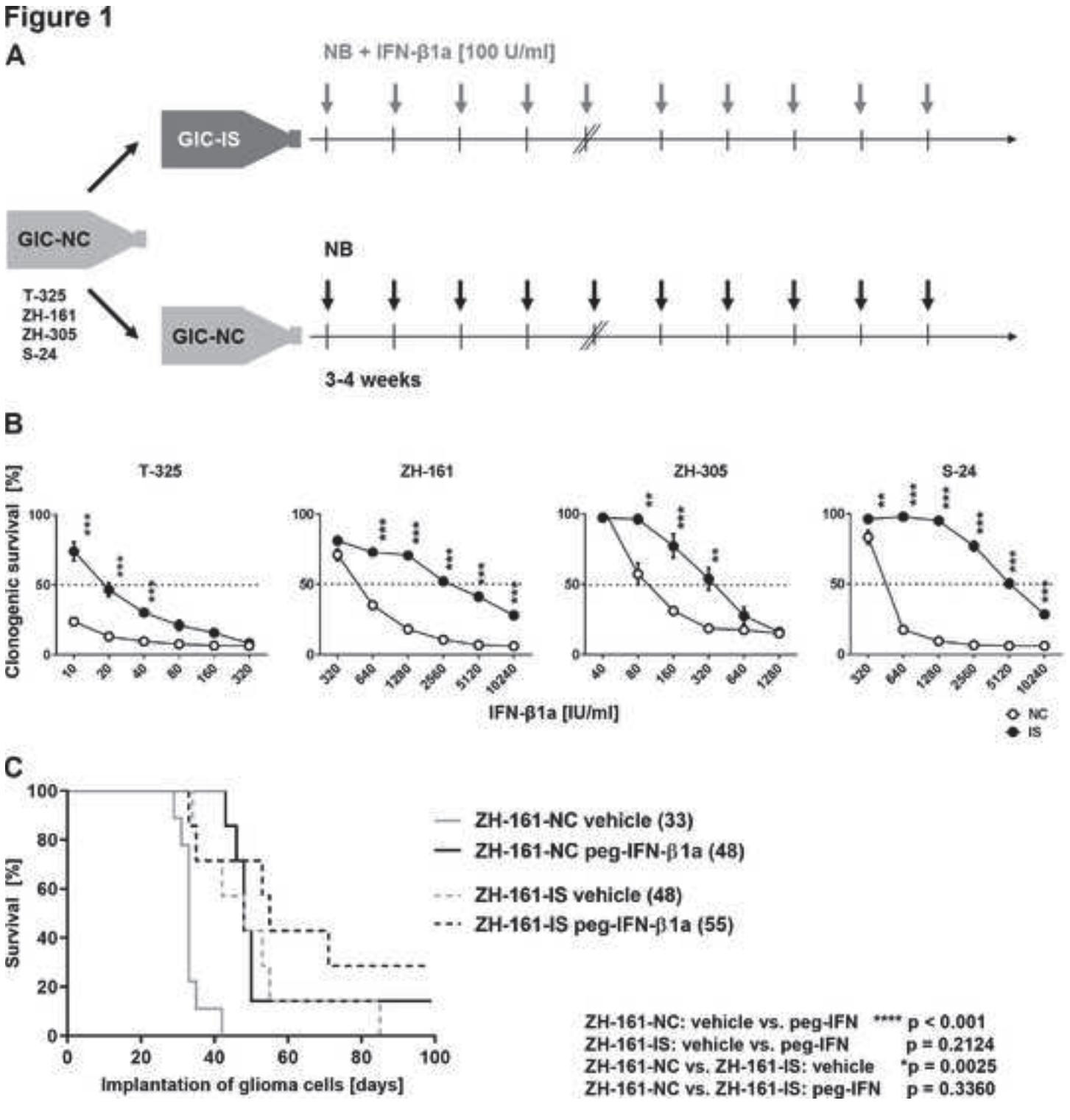
Figure 1
A
NB + IFN-β1a [100 U/ml]
GIC-IS
GIC-NC
NB
T-325
ZH-161
ZH-305
S-24
GIC-NC
3-4 weeks
B
T-325
ZH-161
ZH-305
S-24
Clonogenic survival [%]
IFN-β1a [IU/ml]
NC
IS
C
Survival [%]
Implantation of glioma cells [days]
ZH-161-NC vehicle (33)
ZH-161-NC peg-IFN-β1a (48)
ZH-161-IS vehicle (48)
ZH-161-IS peg-IFN-β1a (55)
ZH-161-NC: vehicle vs. peg-IFN **** p < 0.001
ZH-161-IS: vehicle vs. peg-IFN p = 0.2124
ZH-161-NC vs. ZH-161-IS: vehicle *p = 0.0025
ZH-161-NC vs. ZH-161-IS: peg-IFN p = 0.3360

Click here to access/download;Figure;80-L Figure 2.tif

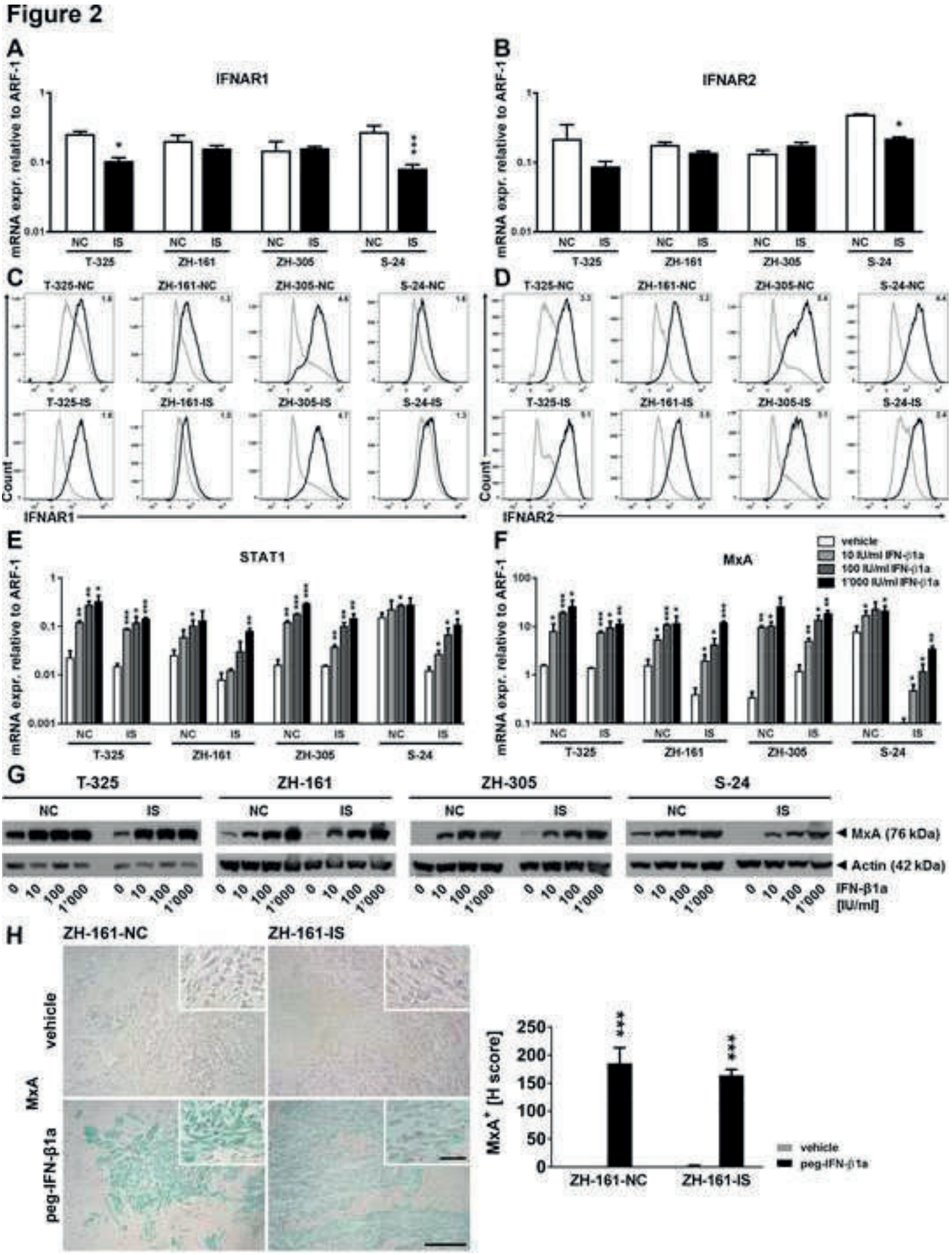

Click here to access/download;Figure;80-L Figure 3.tif

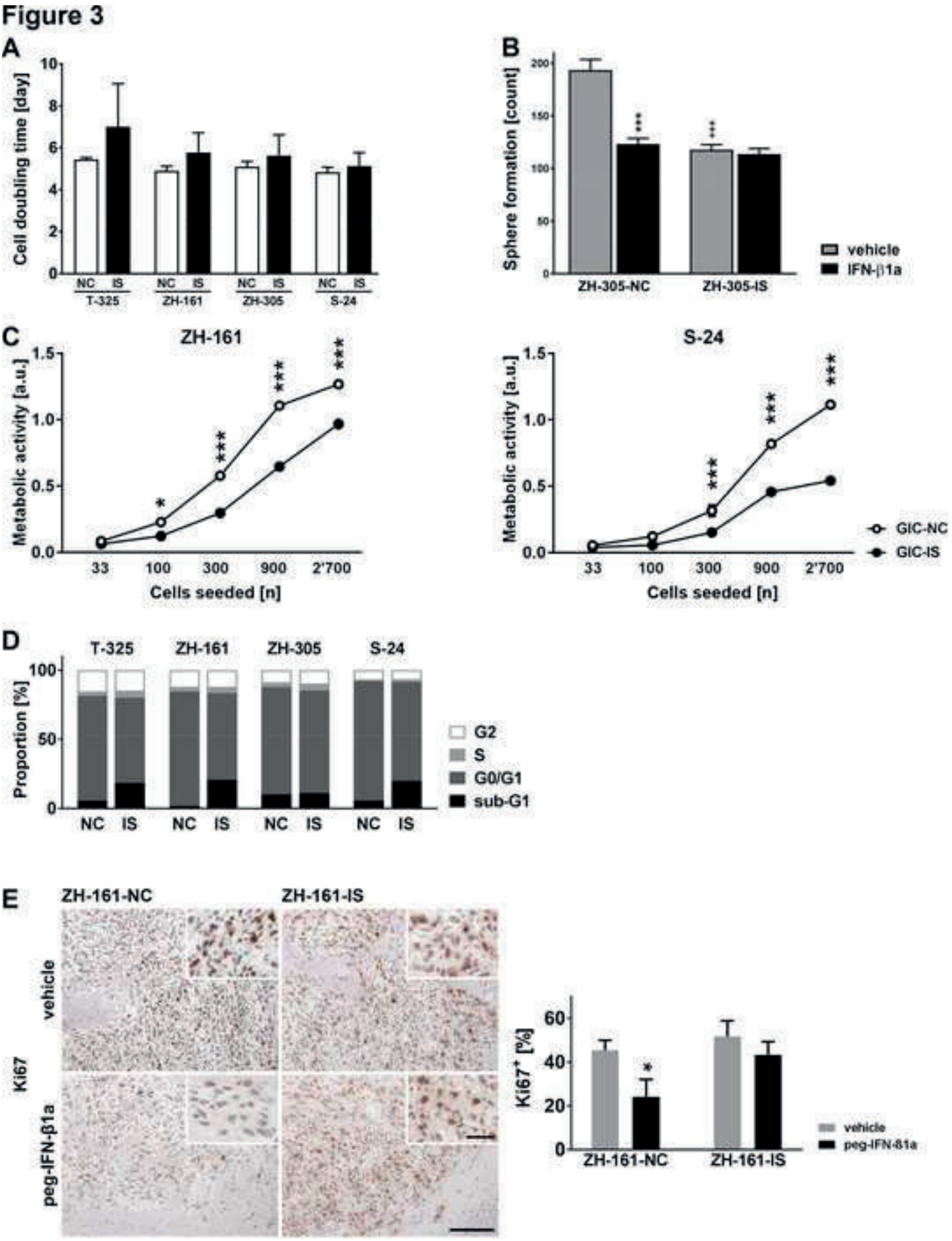

Click here to access/download;Figure;80-L Figure 4.tif

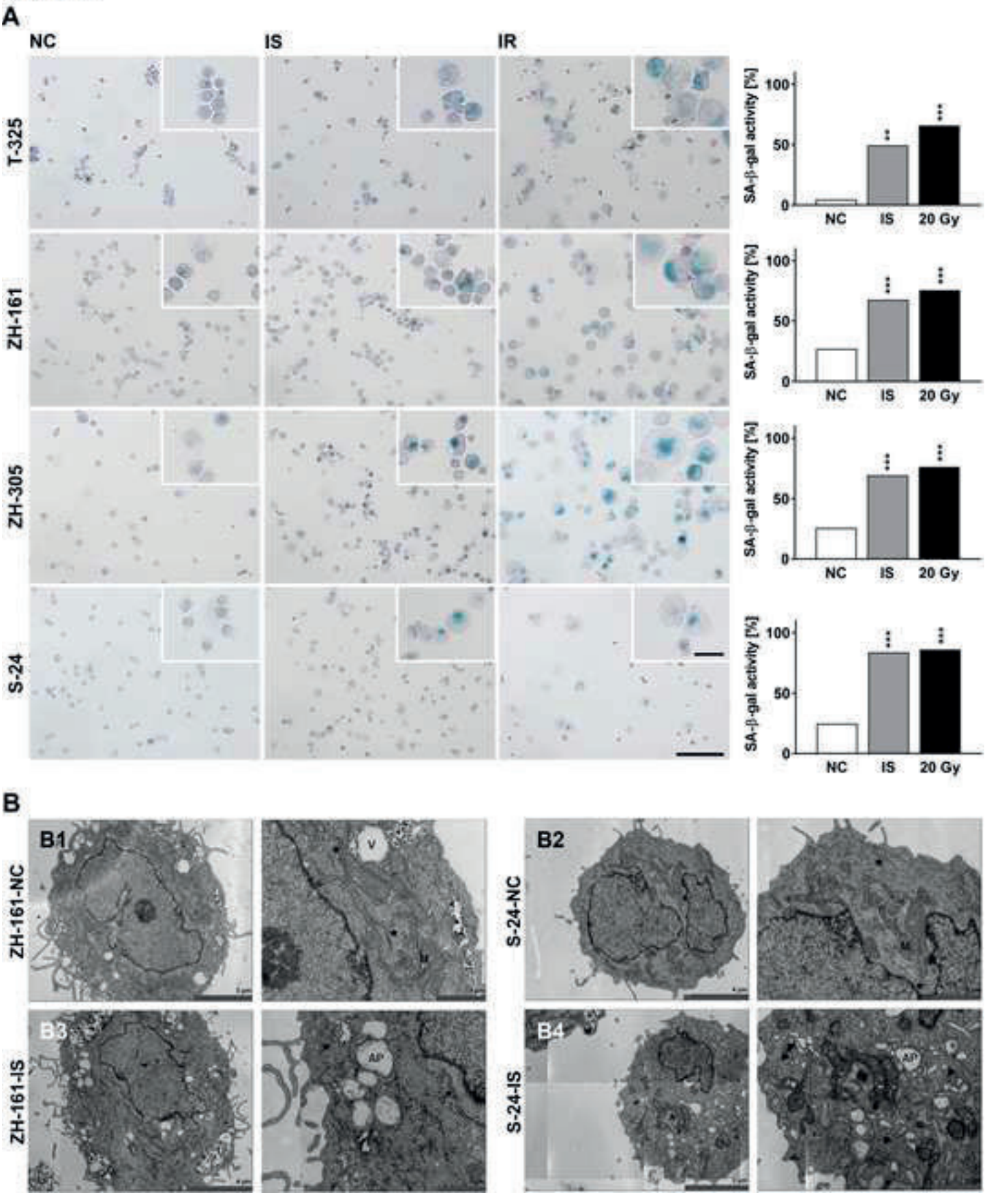

Click here to access/download;Figure;80-L Figure 5.tif

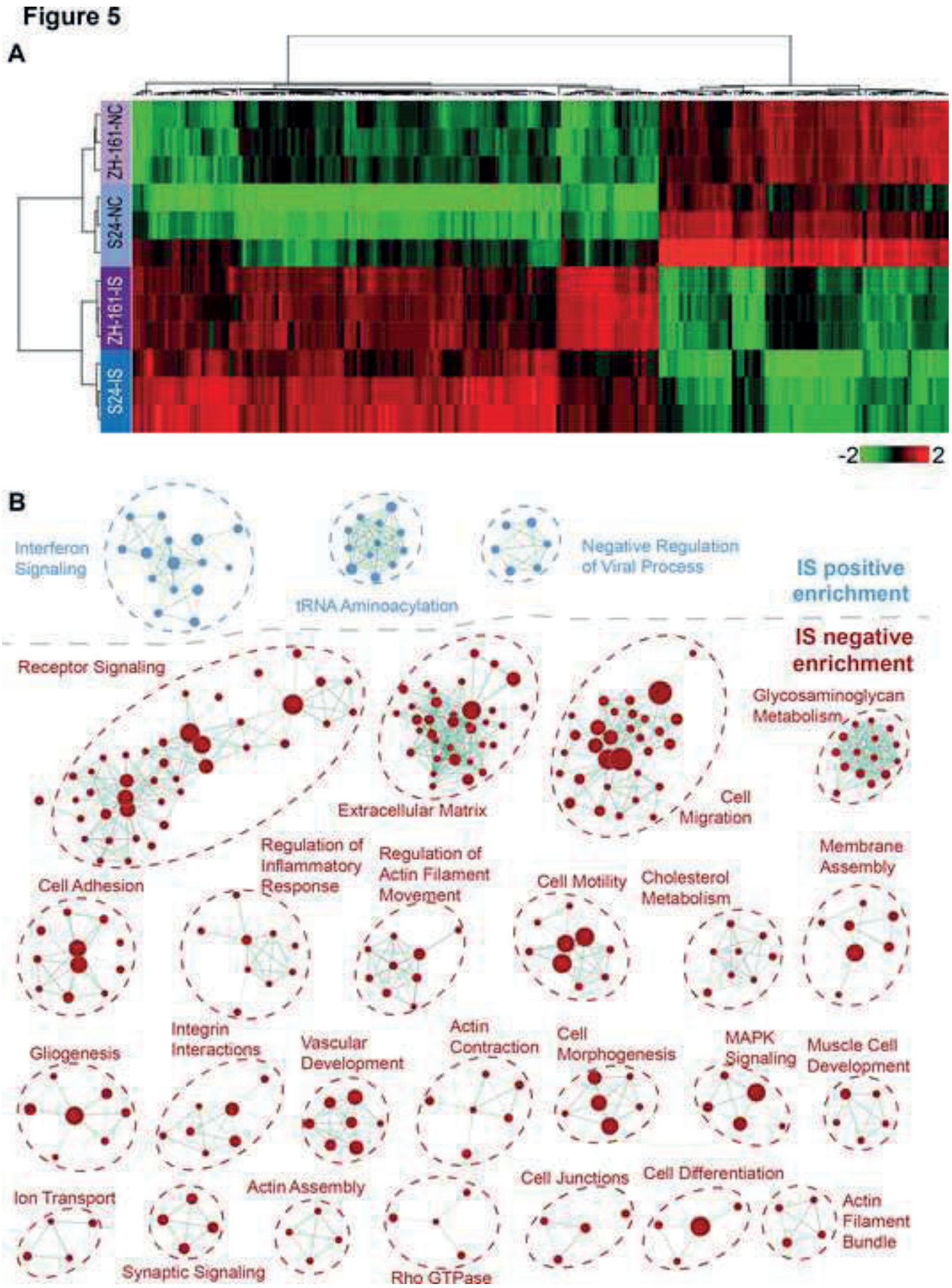

Click here to access/download;Figure;80-L Figure 6.tif

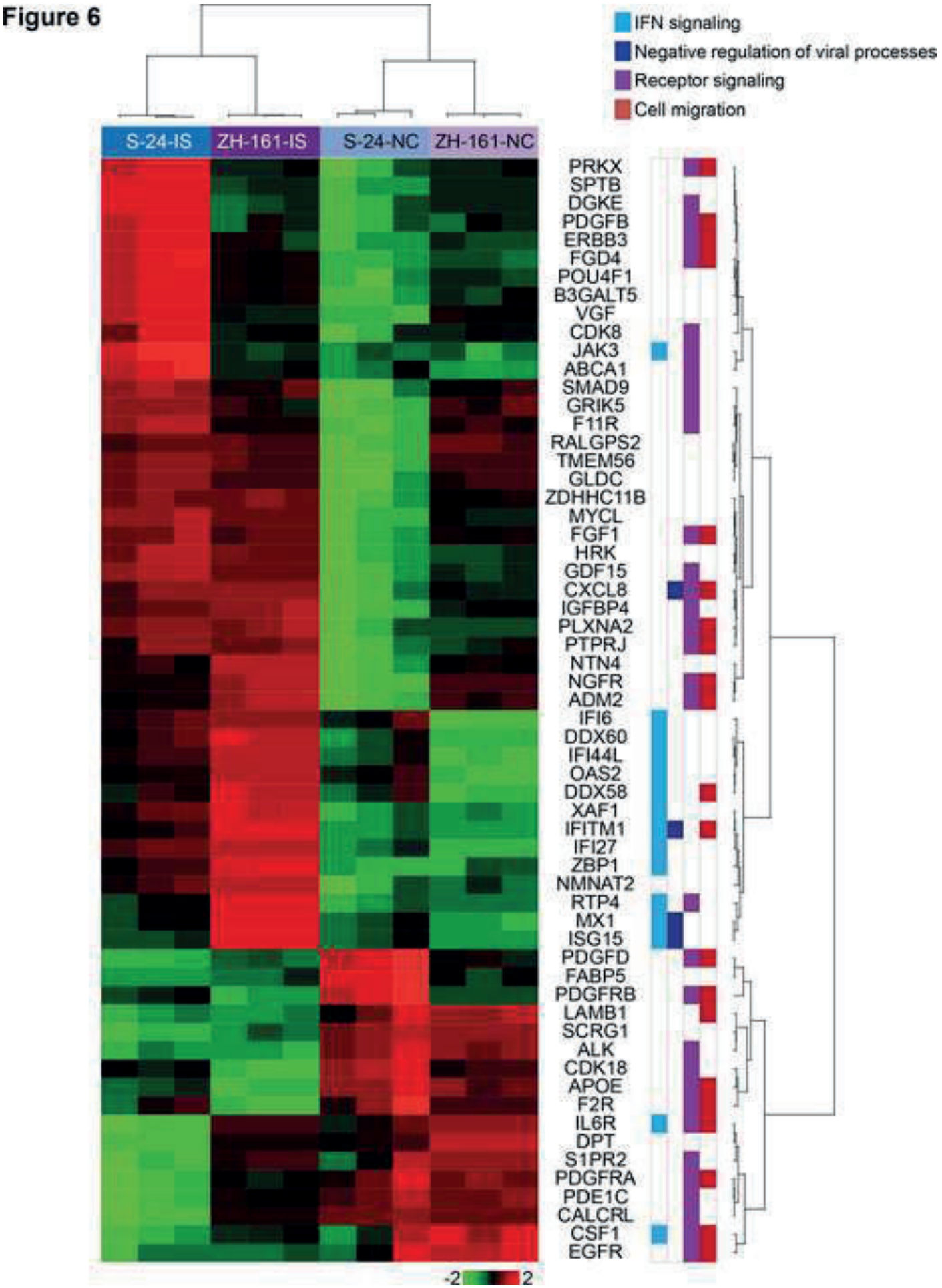

Supplementary Note 1

Real-time (RT) PCR

Total mRNA for baseline gene expression analyses was extracted from human GIC after 24 h incubation in serum-free medium. Gene expression was measured using the Real Time PCR System QuantStudio 6 (Thermo Fisher Scientific) with PowerUp SYBR™ Green Master Mix (Thermo Fisher Scientific) and primers at optimized concentrations. The conditions for RT-PCR were 40 cycles, 95°C/15 sec, 60°C/1 min, 72°C/30 sec. Relative quantification of gene expression was determined by comparison of threshold values. Specific target gene expression was normalized to the housekeeping gene hypoxanthine phosphoribosyltransferase 1 (HPRT1) or ADP-ribosylation factor 1 (ARF1) and calculated with the ΔCT-method for relative quantification with respect to primer efficiency calculated by the standard curve method. The following, human-specific primers were used: ARF1 (forward 5'-GACCACGATCCTCTACAAGC-3', reverse 5'-TCCCACACAGTGAAGCTG-3'), HPRT1 (forward 5'-TGAGGATTTGGAAAGGGTGT-3', reverse 5'-AGCACACAG AGGGCTACAA-3'), IFNAR1 (forward 5'-TATGCTGCGAAAGTCTTCTTGAG-3', reverse 5'-TCTTGGCTAGTTTGGGAACT GTA-3'), MxA (forward 5'-TGGAGATCAG-CTCCCGAGATG-3', reverse 5'-ATTGCCCACAGCCACTCTG-3'), anaplastic lymphoma kinase (ALK (forward 5'CCTGGAGCTGGTCATTACGA-3', reverse 5'-TGGTTTGTGAAGGAGCCATT-3') (all Microsynth, Balgach, Switzerland), IFNAR2 (Bio-Rad, qHsaCED0045841) and NGFR (Bio-Rad, qHsaCEP0054030).

Immunoblot

For immunoblot analysis, whole cell lysates were prepared using RIPA lysis buffer (Merck & Cie, Zug, Switzerland) containing 1% NP-40, 0.5% sodium deoxycholate,

50 mM Tris-HCl pH 8.0, 150 mM NaCl, 5 mM EDTA pH 8.0, 0.1% SDS in Milli-Q water supplemented with 2 µg/mL aprotinin (Sigma Aldrich, St. Louis, MO), 10 µg/mL leupeptin (Sigma Aldrich), 100 µg/mL phenylmethylsulfonyl fluoride (Sigma Aldrich), and phosphatase inhibitor cocktails 2 and 3 (Sigma Aldrich). Protein levels were determined using the BCA Protein Assay Kit (Thermo Fisher Scientific). SDS-PAGE (10% acrylamide gels) was performed with loading of equal protein amounts per lane, then proteins were transferred to nitrocellulose membranes (BioRad, Hercules, CA). Membranes were blocked in Tris-buffered saline containing 5% skim milk or 5% bovine serum albumin (Applichem Panreac, Darmstadt, Germany) and 0.1% Tween 20 (Serva, Heidelberg, Germany) and incubated with the following antibodies: IFNAR1 (LifeSpan BioSciences Inc., Seattle, WI, LS-C185508, 1:500), MxA hybridoma supernatant (provided by J. Pavlovic, Zurich, Switzerland, clone 143, 1:5), ALK (Cell Signaling, Denvers, MA, D5F3, 1:2’000) or β-actin (Santa Cruz Biotechnology, Heidelberg, Germany, sc1616, 1:1’000). Secondary antibodies were Amersham ECL mouse IgG-HRP (GE Healthcare Lifesciences, Glattbrugg, Switzerland, NA931V, 1:3’333), donkey anti-goat IgG-HRP (Santa Cruz Biotechnology, sc-2033, 1:3’333), or goat anti-rabbit IgG-HRP (Santa Cruz Biotechnology, sc-2004, 1:3’333).

Flow cytometry

The following antibodies were used for flow cytometric analysis: phycoerythrin (PE)-conjugated monoclonal mouse anti-human IFNAR1 (Thermo Fisher Scientific, clone 85228), PE-conjugated monoclonal mouse anti-human IFNAR2 (PBL Assay Science, Piscataway, NJ, USA, clone MMHAR-2), PE-conjugated mouse IgG1κ isotype control (BD Biosciences, Allschwil, Switzerland, clone MOPC-21). Flow cytometry was performed according to standard protocols followed by analysis using a BD FACS

Verse flow cytometer (BD Biosciences). Data analysis was performed using FlowJo Version 10.0.7 (Tree Star, Ashland, OR).

Cell doubling time

To determine the cell doubling time, a single cell suspension of 500 GIC was seeded in a 96-well plate. Every three days, viable cell counts were obtained by counting cells using trypan blue solution (dead cell exclusion) and a Neubauer chamber. To calculate the average time it takes for a cell population to double in the exponential phase, the following formula was used: $\frac{duration * \log(2)}{\log(Final\ Concentration) - \log(Initial\ Concentration)}$ [1].

Cell cycle analysis

Cells were fixed and permeabilized with ice-cold 70% ethanol for 30 min. RNA was digested with RNase A (Gibco) and DNA was stained with PI (Sigma-Aldrich). Cells were analyzed using FACS Verse (BD Biosciences).

Spherogenicity assays

Spherogenicity assays were performed by seeding 1’000 cells per well in 96-well plates which were allowed to recover overnight in NB medium. Subsequently, the cells were exposed to human IFN-β1a at different concentrations in NB medium. The assays were continued by an observation period for more than ten days. Either the metabolic activity as a surrogate marker of sphere formation was assessed by MTT assay or spheres, defined as clusters of more than five cells, were counted under the microscope and pictures were taken at days 0, 5, 10, 15 and 20. In some experiments, cells were pretreated with IFN-β1a for 24 h and then exposed to single fraction irradiation or temozolomide as described[2].

Limiting dilution assay

For the limiting dilution assay, single cell suspensions with different densities of GIC were seeded in NB medium in 96-well plates. The assays were stopped after more than ten days and metabolic activity was assessed by MTT assay.

Senescence staining

Senescence was investigated using the Senescence β-Galactosidase Staining Kit (Cell Signalling, Leiden, The Netherlands). Irradiated (20 Gy) and non-irradiated GIC-NC as well as non-irradiated GIC-IS were centrifuged on microscope slides. After fixation with fixative solution for 15 min at room temperature, cells were incubated with β-galactosidase staining solution in order to detect β-galactosidase activity at pH 6 for two to four days at 37°C without CO_2. As soon as blue coloration was observed under the microscope (20x magnification), cells were covered with 70% glycerol for long-term storage.

Transmission electron microscopy

10^5 cells in NB medium were fixed in 2.5% glutaraldehyde in 0.1 M sodium cacodylate buffer, assimilated in cellulose capillaries, dehydrated in ethanol, embedded in epon araldite and cut into 70 nm sections. Irradiated (20 Gy) and cycloheximide (CHX)-treated [10 µg/ml, 15 h] (Santa Cruz Biotechnology) cells were included as controls. Microscopy was performed using a Tecnai Spirit transmission electron microscope (FEI, Hillsborough, OR) [3].

Immunofluorescence

Cells (2.5×10^5) were spun onto glass slides, dried for 30 min, fixed in 4% formaline for 20 min and permeabilized with 0.1% Triton X100. Subsequently, cells were

stained using the polyclonal rabbit anti-golgin 97 (Abcam, Cambridge, UK, ab84340, 1:180) or monoclonal rabbit anti-calnexin (Abcam, ab92573, clone ID: EPR3632, 1:1’000) primary antibody, visualized using an Alexa Fluor 488 or 594-conjugated secondary antibody, respectively (Southern Biotech), and mounted in Dako Fluorescent Mounting Medium (Dako) with 4′,6′-diamidino-2-phenylindole (DAPI) (Thermo Fisher Scientific). Cells were visualized using the SP5 confocal microscope (Leica Microsystems, Heerbrugg, Switzerland). In parallel experiments, NC or IS cells were incubated with 100 nM MitoTracker® Red CMXRos (Cell Signalling) for 30 min at 37°C. After incubation, the cells were spun onto glass slides and fixed with 4% formaline for 20 min. Cell nuclei were stained with DAPI (Thermo Fisher Scientific) and cells were mounted with Dako Fluorescent Mounting Medium (Dako). Cells were analyzed using the SP5 confocal microscope (Leica Microsystems).

Protein synthesis assay

Cells were incubated with O-propargyl-puromycin for 60 min at 37°C, then fixed in cell-based assay fixative for 5 min and washed three times for 5 min. Cells were stained with 5 FAM-azide staining solution for 30 min at room temperature in the dark, washed three times, resuspended in assay buffer and spun onto glass slides (Protein Synthesis Assay Kit, Cyman Chemical Company). O-propargyl-puromycin incorporates into the C-terminus of translated polypeptide chains and thus stops the translation. The truncated chain can be detected by FAM-azide. Cells were examined using the SP5 confocal microscope (Leica Microsystems). CHX-treated cells [10 µg/ml, 15 h] were included as controls to demonstrate impaired protein synthesis.

Supplementary Note 2

Immunohistochemistry

Cryosections were fixed in 4% formaline or acetone for 10 min, pre-treated with 3% H_2O_2 and blocked with blocking reagent A+B (Nichirei Biosciences Inc., Tokyo, Japan, Kit 414321) for MxA staining or with blocking solution (Candor Biosciences, Wangen, Germany) for all other stainings. After blocking, the primary antibodies were applied overnight at 4°C. Primary antibodies were MxA hybridoma supernatant (provided by J. Pavlovic, Zurich, Switzerland, clone 143, 1:5), monoclonal rat anti-CD31 (BD Biosciences, 550274, clone ID: MEC13.3, target antigen: 129/Sv mouse-derived endothelioma cell line tEnd.1, 1:50), monoclonal rabbit anti-Ki-67 (Epitomics, Burlingame, 4203-1, RRID:AB_76s5010, target antigen: human Ki-67, clone ID: SP6, 1:100) and monoclonal mouse anti-Sox-2 (Abcam, ab171380, target antigen: human Sox-2, clone ID: 20G5, 1:200). Secondary antibodies were incubated for 10-30 min at room temperature. Histofine Simple Stain human and mouse MAX PO secondary-labelled antibody systems were obtained from Nichirei Biosciences Inc. The antigen antibody conjugates were detected by staining with DAB (Dako Baar, Switzerland) for 1-3 min or Green HRP (Dako) for 5-10 min. Nuclei were counterstained using hematoxylin for 1-4 min, washed in water and dehydrated twice in 96% ethanol, then twice in 100% ethanol and three times in Roticlear (Carl Roth, Karlsruhe, Germany) before mounting onto coverslips using Rotimount mounting medium (Carl Roth). Quantification of immunohistological stainings was obtained from four regions of interest from three tumors per group. Within tumor tissues, percentages of Ki-67-positive cells of all nucleated cells were determined, microvessel density was calculated by counting $CD31^+$ capillaries per tumor ROI. Tumor volumes were calculated using an approximation based on ellipsoid geometric primitive [4]. Satellite lesions defined as tumor cell aggregates >10 cells and at least three cell layers distant from the main tumor bulk were counted on H&E-stained sections.

References

1. Roth V. Doubling Time Computing. 2006; www.doubling-time.com/compute.php.

2. Happold C, Roth P, Silginer M, et al. Interferon-beta induces loss of spherogenicity and overcomes therapy resistance of glioblastoma stem cells. *Molecular cancer therapeutics.* 2014; 13(4):948-961.

3. Silginer M, Nagy S, Happold C, Schneider H, Weller M, Roth P. Autocrine activation of the IFN signaling pathway may promote immune escape in glioblastoma. *Neuro Oncol.* 2017; 19(10):1338-1349.

4. Schmidt KF, Ziu M, Schmidt NO, et al. Volume reconstruction techniques improve the correlation between histological and in vivo tumor volume measurements in mouse models of human gliomas. *Journal of neuro-oncology.* 2004; 68(3):207-215.

Figure S1

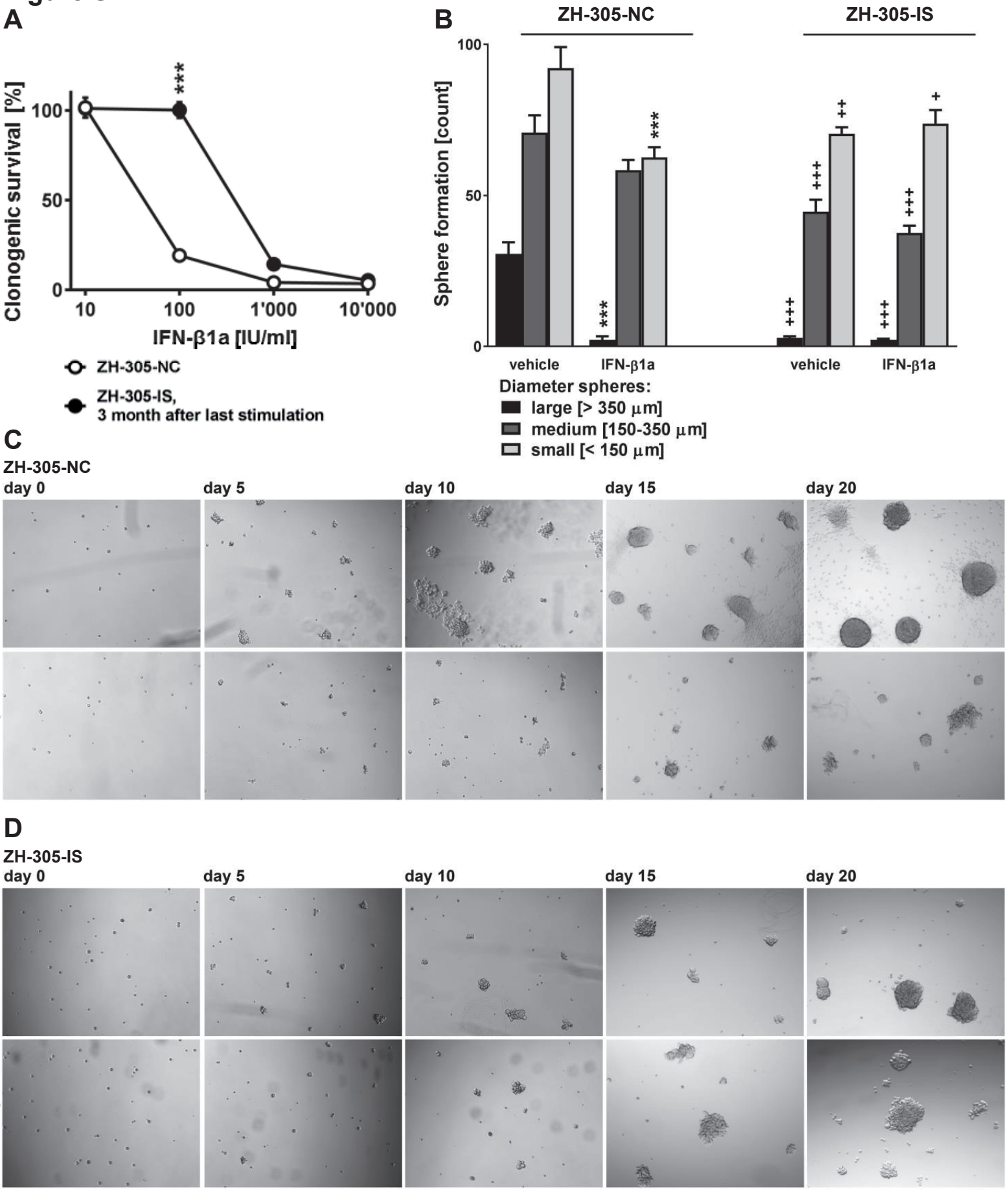

Figure S1. **Sphere formation capacity of ZH-305-NC and ZH-305-IS *in vitro*.** A. Clonogenic survival of ZH-305-IS versus ZH-305-NC after a wash-out period of IFN-β1a of three months. B-D. Time-dependent responsiveness to IFN-β1a [100 IU/ml| was determined by obtaining counts for spheres of different sizes on day 20 (B) and by morphological studies of ZH-305-NC (C) and ZH-305-IS (D) at 0, 5, 10, 15, and 20 days. Data in A,B are expressed as mean and SEM (one way ANOVA with Tukey's post-hoc test for multiple analysis, A ***p<0.001 ZH-305-IS versus ZH-305-NC, B ***p<0.001 IFN-β1a-treated versus untreated NC cells, $^{+++}$p<0.001 IS versus NC cells).

Figure S2

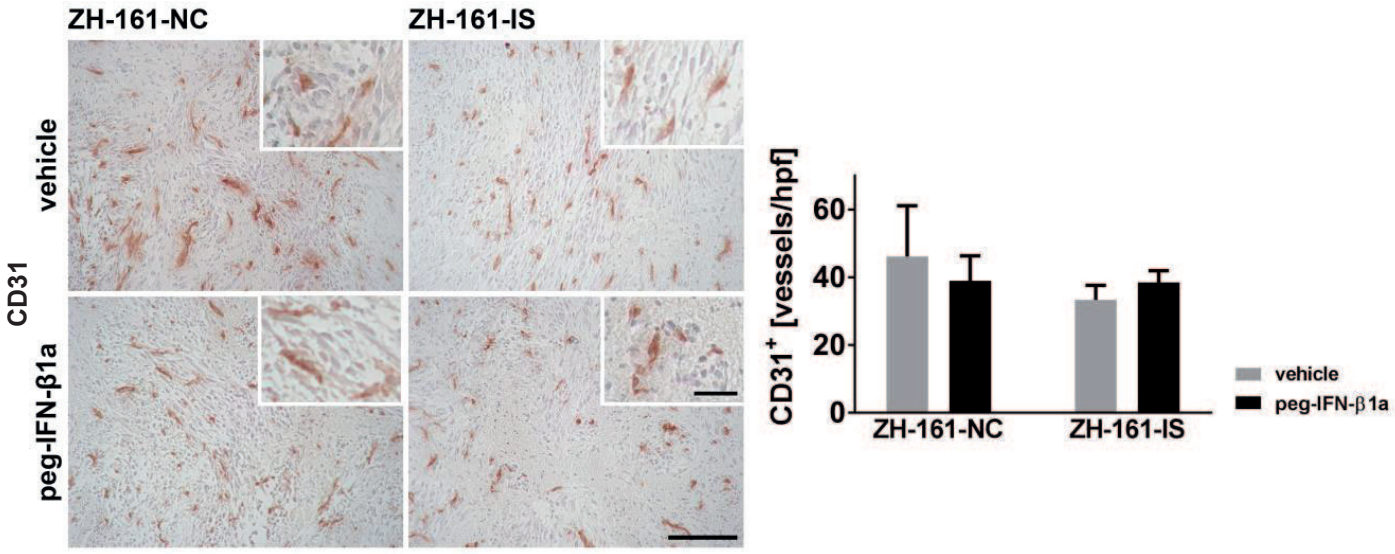

Figure S2. **No effects on angiogenesis of peg-IFN-β1a in xenograft glioma mouse models of ZH-161-NC versus ZH-161-IS.** Nude mice intracranially implanted with ZH-161-NC or ZH-161-IS cells were treated twice weekly with vehicle or peg-IFN-β1a [$8x10^7$ U/kg] from day 14 on. Vessel density was determined by counting CD31+ capillaries in four ROI per tumor of early stage tumors. Data are expressed as means and SEM. Scale bars of full pictures correspond to 100 µm, scale bars of inserts to 25 µm.

Figure S3

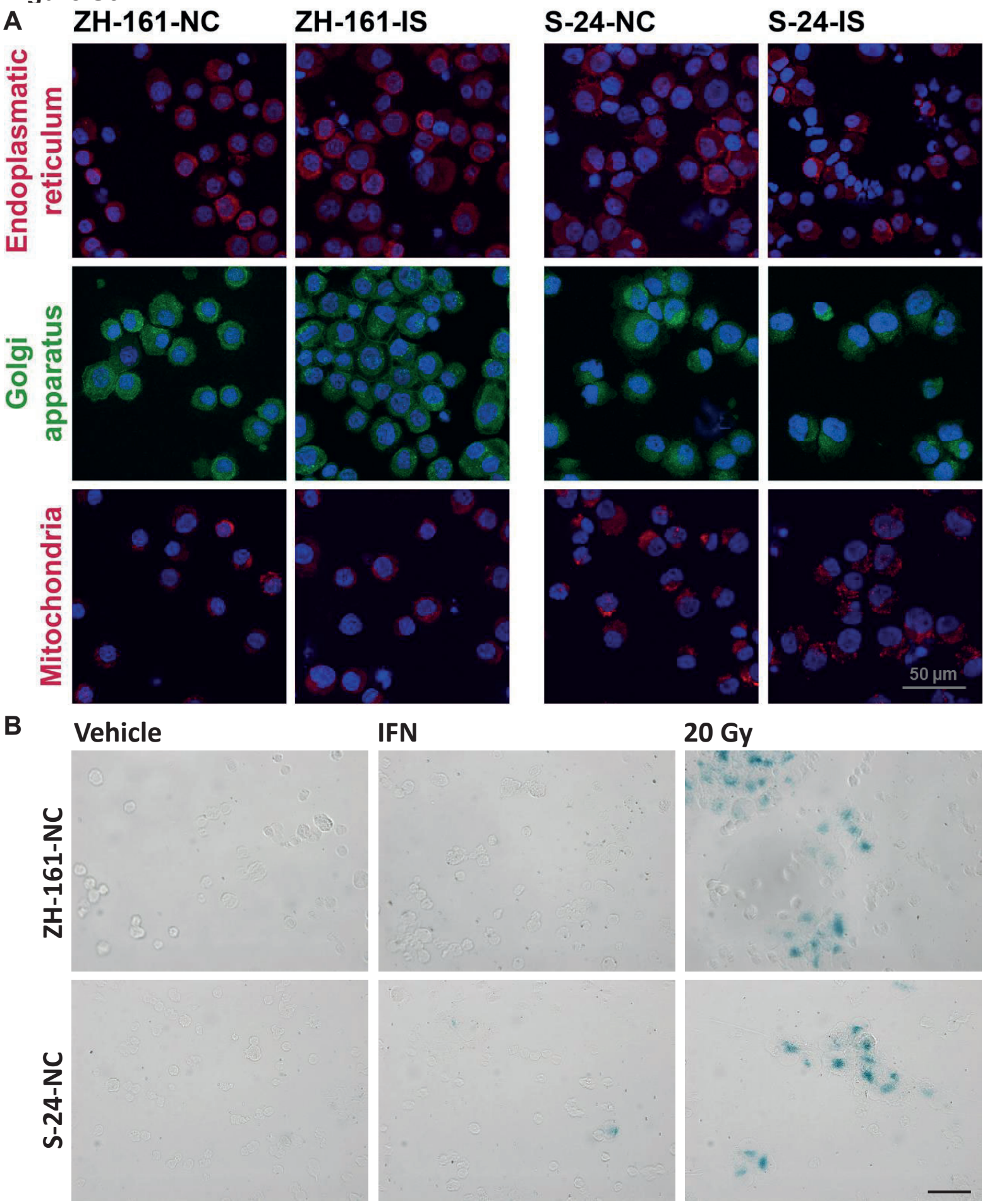

Figure S3. **Morphological characterization of IS cells.** A. Immunofluorescence stainings of the endoplasmatic reticulum (red), golgi apparatus (green) and mitochondria (red) of ZH-161 and S-24 NC and IS cells. Cell nuclei are stained with DAPI (blue). B. Senescence-associated β-galactosidase staining on cytospins of NC cells stimulated with IFN-β1a (100 IU/ml) for 24 h. Scale bars of full picture corresponds to 50 µm.

Figure S4

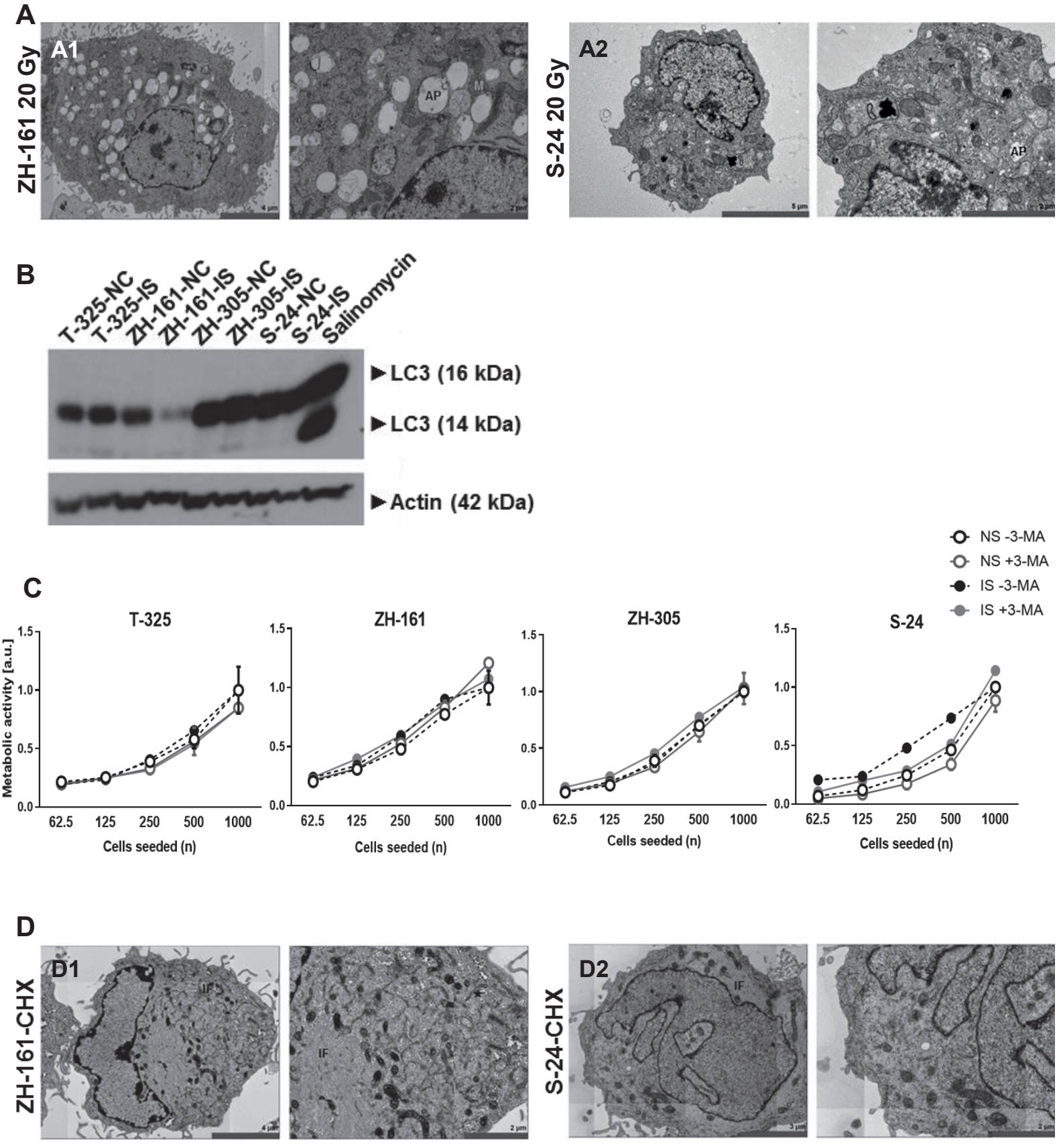
A
ZH-161 20 Gy
A1
AP
M
S-24 20 Gy
A2
AP
B
T-325-NC
T-325-IS
ZH-161-NC
ZH-161-IS
ZH-305-NC
ZH-305-IS
S-24-NC
S-24-IS
Salinomycin
LC3 (16 kDa)
LC3 (14 kDa)
Actin (42 kDa)
C
NS -3-MA
NS +3-MA
IS -3-MA
IS +3-MA
T-325
ZH-161
ZH-305
S-24
Metabolic activity [a.u.]
0.0
0.5
1.0
1.5
62.5
125
250
500
1000
Cells seeded (n)
D
ZH-161-CHX
D1
IF
S-24-CHX
D2
IF

Figure S4

E

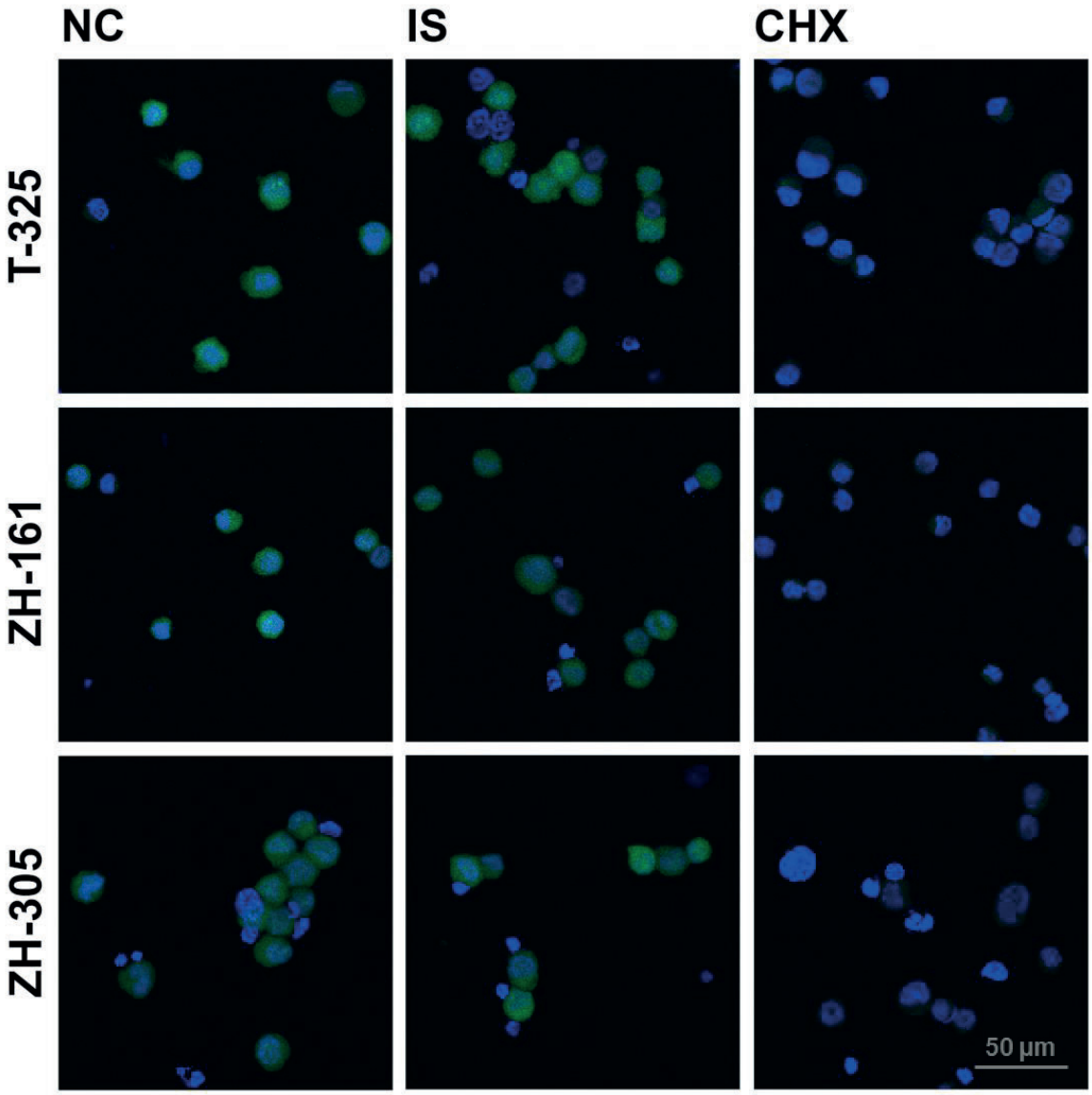

Figure S4. **Ultrastructural characterization of IS cells.** A. Transmission electron microscopy data of irradiated (20 Gy) ZH-161 and S-24 NC cells. Representative pictures of 70 nm sections are shown. AP = autophagosome (A1, A2), M = swollen mitochondria (A1). B. Protein accumulation of LC3 in NC and IS cells assessed by immunoblot. Actin served as loading control. C. Sphere formation of ZH-161 and S-24-NC (white) or IS (black) cells after seeding different cell densities without or with 3-methyladenine (1 mM) treatment. Metabolic activity was assessed by MTT assay . D. Transmission electron microscopy data of cycloheximide (CHX, 10 µg/ml, 15 h)-treated ZH-161 and S-24 NC cells. IF = intermediate filaments (D1, D2). E. Fluorescently labelled NC and IS cells capable of synthesizing proteins (green). Cell nuclei are stained with DAPI (blue). CHX-treated NC cells (10 µg/ml, 15 h) served as negative control.

Figure S5

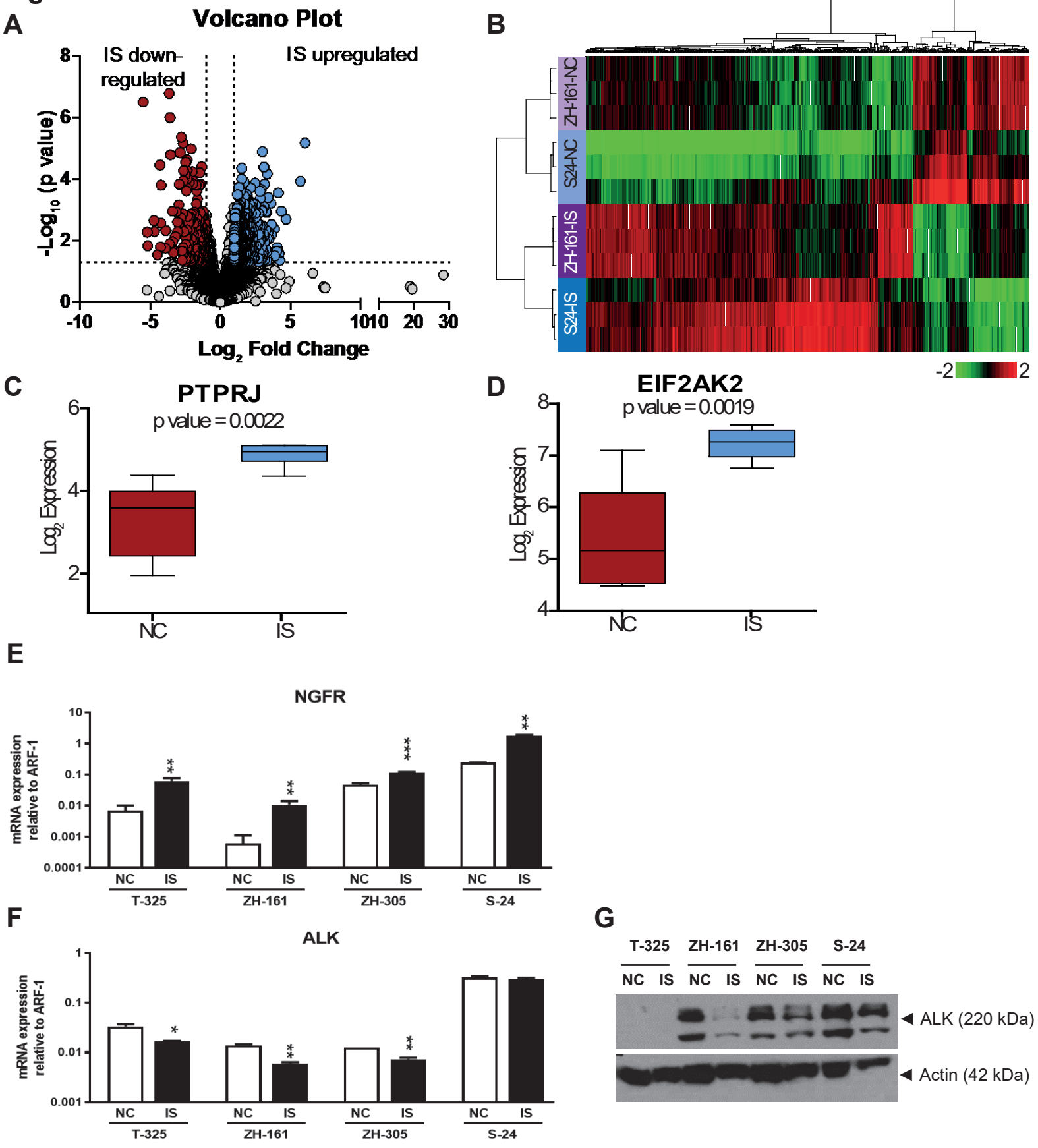

Figure S5. **Altered gene expression in IS models.** A. Volcano plot of altered gene regulation in ZH-161-IS and S-24-IS cells validated by RNA sequencing. B. Unsupervised clustering of 783 significantly regulated genes between IS and NC cells. Upregulated genes are indicated in red, downregulated genes in green (Z score +/- 2). C,D. PTPRJ or EIF2AK2 expression of ZH-161 and S-24 IS versus NC cells determined by RNA sequencing. Data are expressed as mean and SEM. E,F. Relative mRNA expression of NGFR (E) or ALK (F) analyzed in IS versus NC cells by RT-PCR. ARF-1 served as housekeeping gene (**p<0.01, ***p<0.001, one way ANOVA with Tukey's post hoc test for multiple analysis, IS versus the corresponding NC cell line). G. ALK protein levels in NC and IS cells were assessed by immunoblot. Actin served as loading control.

Figure S6

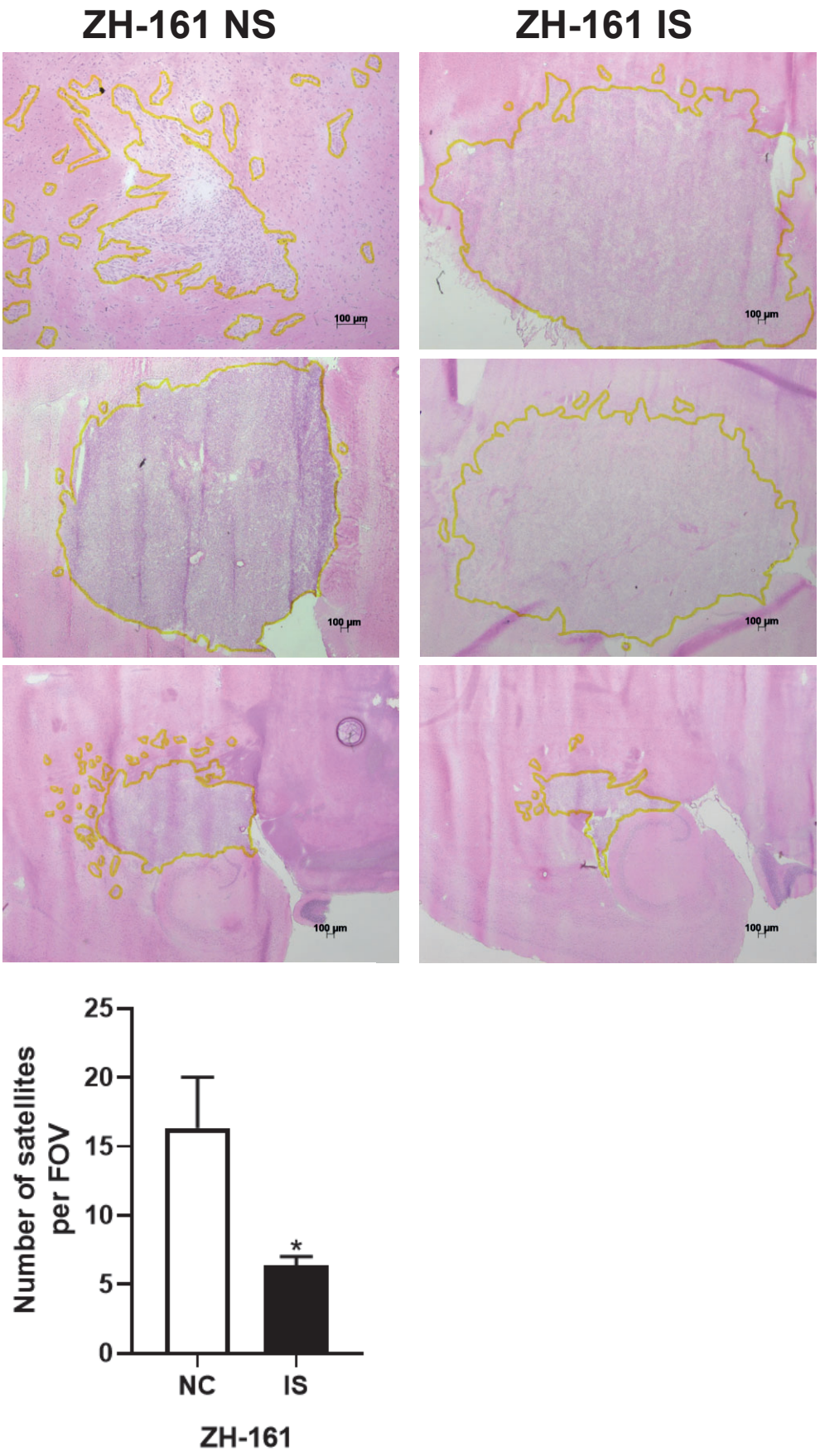

Figure S6. **ZH-161 IS cells form less invasive tumors than ZH-161 NC cells.** Brain sections of ZH-161-NC or ZH-161-IS tumor-bearing animals sacrificed when the third mouse became symptomatic, were analyzed histologically to assess the mean number of invasive satellites per section. Representative images of hematoxylin and eosin-stained tumors with tumor borders highlighted in yellow. Results are expressed as means and SEM of the number of satellites per fiels of vision (FOV) of n=3 tumors per group.